Strong Field Approximation for High Order Harmonic Generation with $\omega/2\omega$ Laser Fields

J. Marcus Dahlström

Lund Reports on Atomic Physics, LRAP-381
Lund, June 2007

Abstract

The aim of this Thesis is to investigate high order harmonic generation in presence of a two color driving field. A dilute rare gas is exposed to the output of a Titanium Sapphire laser mixed with its second harmonic. This quantum mechanical process is calculated in MATLAB using the Strong Field Approximation. The single atom response to fields of both few and many cycles is computed.

The results show that the high harmonic generation process can be improved significantly using a two color field. The output intensity can be increased and tuned to specific central frequencies. The results also show that the duration of single attosecond bursts can be reduced by a factor of two. It is, however, not possible to combine amplification and temporal compression in the output. The calculations show good agreement with recent experiments in Lund.

Deeper insight into the spectral features of the two color high order harmonic generation has been gained using the Feynman Path Integral formalism. These predictions have been verified by simulations in Matlab.

Populärvetenskaplig sammanfattning

Övertonsgenerering är ett fascinerande fenomen som inträffar då intensivt ljus samverkar med materia. Ljuset som används i experimentet består av en laserpuls som komprimeras till så kort längd som möjligt för att optimera intensiteten. Laserpulsen består därför endast av ett fåtal svängningar och dess längd motsvarar ungefär 10 femtosekunder för en infraröd puls. Då laserpulsen fokuseras på en atom blir den resulterande kraften så stor att den tillfälligt löser upp banden mellan elektronerna och kärnan. En elektron kan då slungas ut på en lång färd i den fria rymden. I nästa ögonblick byter laserpulsen riktning på sitt elektriska fält. Elektronen bromsas därför in och sedan dras den tillbaka mot kärnan. Banden mellan elektronen och kärnan bildas på nytt och den överblivna energin sprutar ut i form av en extremt kort ljusblixt. Längden på blixten är cirka 100 attosekunder, vilket är hundra gånger kortare än den komprimerade laserpulsen.

Genom att utnyttja *två* laserpulser med *olika* färger kan man påverka och kontrollera övertonsgenereringen. Kvantmekaniska beräkningar visar att man på detta sätt kan öka intensiteten på de genererade blixtarna och att man kan styra blixtarnas energier. Detta öppnar för praktiska tillämpningar och mer precisa experimentalla metoder.

Contents

Chapter 1

Introduction

1.1 Nonlinear Optics in a Nutshell

An atom consists of a small nucleus and a bunch of orbiting electrons. When an electric field is applied to the atom, the nucleus will be pulled in the direction of the electric field, and the electrons will be pulled in the opposite direction. The result of this relative displacement, is a small dipole moment which creates an electric field opposite to the applied field [1]. The dipole moment increases when the applied field strength increases, but the increase is not linear, because the forces keeping the atom together are not linear.

Matter is made up of many atoms and therefore responds in a similar way. When matter interacts with strong laser fields, the polarization of the material will be nonlinear. This nonlinearity can be taken into account by expanding the susceptibility of the material in a power series:

$$P(t) \equiv P^{(1)}(t) + P^{(2)}(t) + ... = \epsilon_0(\chi^{(1)}E(t) + \chi^{(2)}E^2(t) + ...),$$

where $P(t)$ is the total polarization, $\chi^{(n)}$ is the n'th order susceptibility and $E(t)$ is the electric field. Because the polarization now depends on integer powers of the driving field, there will be new frequencies appearing in the emission. Atomic gases have inversion symmetry and can therefore only emit at odd harmonics of the driving field, see Figure 1.1 [2].

1.2 High Order Harmonic Generation (HHG)

The atom can be ionized due to quantum-tunneling when the laser intensity gets even higher (above 10^{18} W/m^2 for 800 nm laser light). The electrons leave the atom and accelerate to high velocities in the laser field. When the laser field changes sign, the electrons will be decelerated, and some may return to the vicinity of the nucleus. These electrons can then recombine with the nucleus and release energetic photons [3]. The generated photons have energies corresponding to odd harmonics of the driving field. The higher the intensity of the driving field is, the higher energy photons can be produced. Qualitatively, there is one important difference between conventional nonlinear optics and high order harmonic generation. In high order harmonic generation, a large number

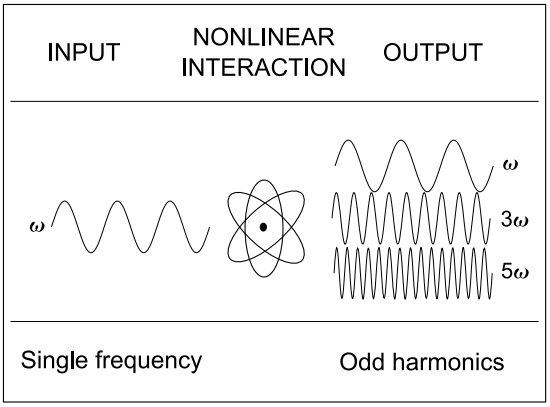

Figure 1.1: Due to the nonlinearity of the interaction with the atom, the output laser beam will include multiples of the input laser frequency. Even harmonics can only be created when there is an time-average dislocation of the electron distribution. Net dislocations can't be created from monochromatic driving fields and atoms with inversion symmetry because the electron will always be at the nucleus on time average.

of harmonics have equal strength, whereas in conventional nonlinear optics the harmonic strength always decreases with the harmonic order.

1.3 Bichromatic Driving Field $\omega/2\omega$

Recent experimental work in Lund have showed that the harmonic intensity can be increased if the generation is driven by two laser fields instead of one, see Figure 1.2. We investigate a particular bichromatic laser field called $\omega/2\omega$, which includes two monochromatic beams: $\omega = 2\pi c/\lambda$, $\lambda = 800$ nm; and 2ω, where ω denotes an angular frequency, c is the speed of light and λ is the corresponding wavelength in vacuum. Optimizing the output intensity is important, because increasing the number of generated photons improves the quality of applications and experiments. The $\omega/2\omega$ field has several other nice features, such as one attosecond pulse per period [5], and in situ measurements of the generated harmonic phases [6].

Single attosecond bursts (> 100 as) can be produced using ultra short driving pulses (< 5 fs) of ω fields [7]. It has been predicted that the driving fields don't have to be as short if $\omega/2\omega$ fields are used instead of ω fields. Experiments with short phase locked $\omega/2\omega$ pulses (12 fs) have recently been carried out by E. Gustafsson, at ETH in Zürich, to verify these predictions. Early results from experiments, with single laser shots (9 fs) and an unlocked absolute phase, imply that single bursts can be obtained [8].

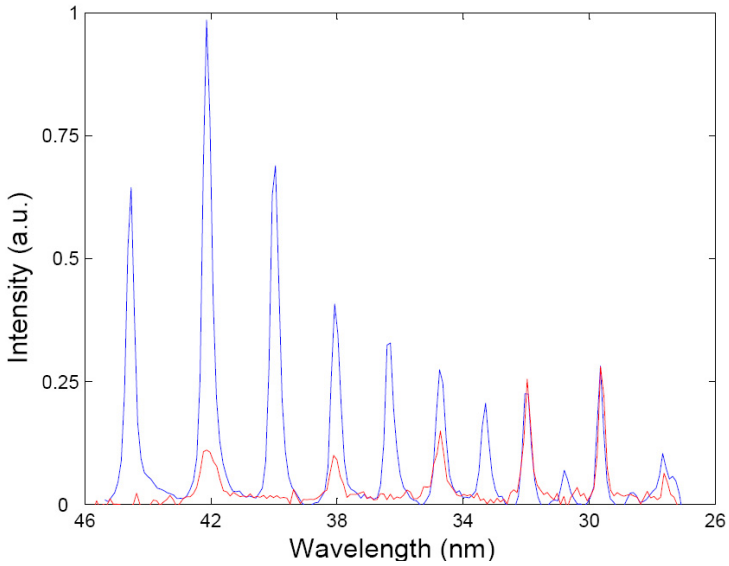

Figure 1.2: The high order harmonic generation from a monochromatic field, ω, consists of odd harmonics (red line). The harmonic intensity decreases fast for wavelengths under 28 nm. This *cut off* energy depends on the intensity of the driving field and it will be discussed in detail in the following chapters. The intensity of the lower harmonics (46-33 nm) can be increased using a two color driving field, $\omega/2\omega$ (blue line). The $\omega/2\omega$ spectrum contains both even and odd harmonics and there are two cut offs: 42 nm and 28 nm, where the latter coincides with the cut off of the ω field [4].

1.4 Aim of Thesis

The aim of this theoretical Thesis is to investigate the high order harmonic generation from $\omega/2\omega$ fields. The duration of the driving pulse is varied from ultra short to continuous. A program, based on the Strong Field Approximation [9], has been written in MATLAB. The program is very general and can be used to calculate the high order harmonic generation of *any* arbitrary low frequency driving field.

Outline of Thesis

The outline of the Thesis is as follows: Chapter 2 explains high order harmonic generation using classical mechanics. A semi-classical picture called the Simple Man's Model [3] is reviewed. The Hamiltonian of the system is constructed and electrodynamic gauge transformations are made to fit the Strong Field Approximation formulation. Chapter 3 covers the limitations of the classical picture. The Feynman Path Integral formulation of quantum mechanics is used to derive a few qualitative results for $\omega/2\omega$ fields. The method described was created by the Author, but the idea that the Feynman Path Integral can be used in combination with high order harmonic generation has been known for a long time [9] [10]. Chapter 4 reviews the Strong Field Approximation, starting from the Schrödinger equation and ends up with an explicit expression for the dipole moment, written with propagator operators. The implementation in MATLAB is then discussed in some detail. Chapter 5 is divided into three parts, where each part contains key results from the MATLAB simulations: A method is described for separating classical trajectories in the Strong Field Approximation; the high order harmonic spectra is studied for a large range of relative intensities of adiabatic $\omega/2\omega$ driving fields; and the $\omega/2\omega$ field is used to improve the attosecond bursts from ultra short driving pulses. Chapter 6 summarizes the results and gives an outlook.

Chapter 2

Classical Trajectories

2.1 Simple Man's Model

High order harmonic generation (HHG) is a quantum mechanical process. It is, however, extremely useful to have worked through the classical problem of a charged particle in an electromagnetic field before dealing with the full complexity of HHG. This semi-classical treatment is often referred to as the Simple Man's Model, see Figure 2.1. In this model, the electron tunnels into the continuum through the atomic potential, which is deformed due to the strong laser field. This tunneling process is illustrated in Figure 2.2. After tunneling into the continuum, the electron is accelerated away from the atom by the laser field. At a later time the laser field changes sign and the electron is pulled back toward the atom. The electron can recombine with the atom and radiate some photons. The photon energy is the sum of the binding potential and kinetic energy of the returning electron due to energy conservation [3].

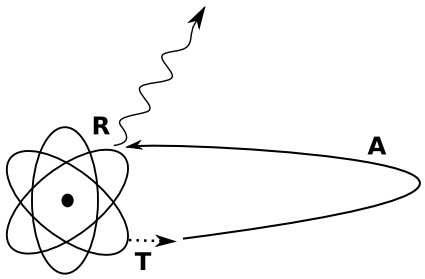

Figure 2.1: In the Simple Man's Model, the electron tunnels at T, accelerates along A and then recombines and generates a photon at R.

2.2 Newtonian Mechanics

Using Newtonian mechanics, particles are accelerated when they are affected by forces. The force acting on a charged particle in an electromagnetic field is

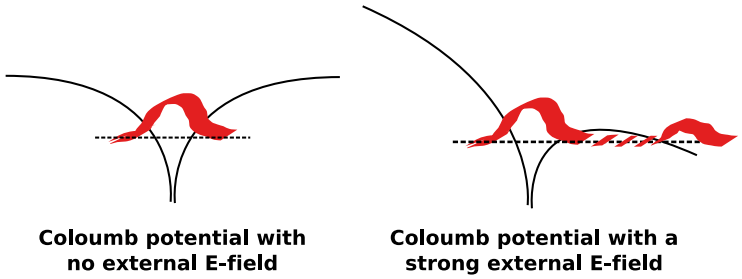

Figure 2.2: The electron is trapped in the Coloumb potential when there is no external E-field (left plot). The electron can tunnel through the Coloumb potential into the continuum when a strong E-field acts on the atom (right plot).

known as the Lorentz force:

$$\vec{F} = q(\vec{E} + \vec{v} \times \vec{B}),$$

$\frac{1}{2}\frac{1}{2}$ where q is the charge and $\vec{v} \equiv \frac{d\vec{r}}{dt}$ is the velocity of the particle, $\vec{E} = \vec{E}(t, \vec{r})$ is the electric field and $\vec{B} = \vec{B}(t, \vec{r})$ is the magnetic field evaluated at the location of the particle, $\vec{r} \equiv \vec{r}(t)$ at time t [1]. The electron in the Simple Man's model is accelerated by a focused femtosecond laser pulse, but the corresponding electromagnetic field is assumed to be a linearly polarized plane wave propagating along the $\hat{z}$-axis in vacuum:

$$\begin{cases} \vec{E}(t, \vec{r}) &= E_0 \sin(\omega t - \vec{k} \cdot \vec{r})\hat{x} \\ \vec{B}(t, \vec{r}) &= -\frac{1}{c}\hat{z} \times \vec{E} \end{cases}$$

where E_0 is the amplitude of the field, $\omega = 2\pi c/\lambda$ is the angular frequency and $\vec{k} = 2\pi/\lambda\ \hat{z}$ is the wave vector [1]. The effective intensity of the driving field $I = c\epsilon_0|E_0|^2/2$ is of the order of 10^{18} W/m^2. The main purpose of the Thesis is to study harmonic generation from two colors laser fields: ω and 2ω, but we start by considering the simpler case with a monochromatic driving field.

The classical trajectories of the electron in the field are completely determined by the initial conditions. We therefore define a tunneling time t' and assume that the electron appears at the origin with zero velocity right after tunneling has occurred:

$$\begin{cases} \vec{r}(t') &= 0 \\ \vec{v}(t') &= \vec{0}. \end{cases}$$

The problem is now fully defined and can be solved by integrating Newton's second law:

$$m\ddot{\vec{r}} = \vec{F} \longrightarrow \vec{r}(t) = \frac{1}{m}\int_{t'}^{t} dt'' \int_{t'}^{t''} dt''' \vec{F}(t''', \vec{r})$$

In the Simple Man's Model only trajectories that return to the origin at some time $t > t'$ are of interest, since these are the only trajectories that can recombine

[1] The laser pulse is a few cycle pulse in reality, but we model it as a continuous wave for simplicity. In this Thesis, we refer to driving pulses as *continuous* if they are longer than 20 fs. Shorter driving pulses (5-20 fs) are referred to as *ultra fast* pulses.

and generate photons. The magnetic field has a small effect on nonrelativistic particle trajectories and can be neglected for the intensities considered in this Thesis. By neglecting the B-field the problem is reduced to one dimension:

$$m\ddot{x} = qE(t) \;\longrightarrow\; x(t) = \frac{1}{m}\int_{t'}^{t} dt'' \int_{t'}^{t''} dt''' qE(t''', x).$$

The IR-field has a very long wavelength compared to the characteristic distance x_{E_c} that the electron travels in a constant E-field E_c during a time $T = \lambda/c$:

$$\frac{\lambda}{x_{E_c}} = \frac{2mc^2}{qE_0\lambda} \approx 46 \gg 1,$$

for an intensity $I = 10^{18}$ W/m^2. This suggests that the dipole approximation can be used, which allows us to neglect the x-dependence in the E-field for trajectories in the Simple Man's Model. The analytical trajectories are calculated for the monochromatic driving field.

$$x(t) = \frac{1}{m}\int_{t'}^{t} dt'' \int_{t'}^{t''} dt''' qE_0 \sin\omega t''' = -\frac{qE_0}{m\omega^2}\sin\omega t + v_D t + x_0,$$

where the drift velocity $v_D = \frac{qE_0}{m\omega}\cos\omega t'$ and the position $x_0 \equiv x(0) = \frac{qE_0}{m\omega}(\frac{1}{\omega}\sin\omega t' - \cos\omega t')$ are integration constants determined by the initial conditions. The kinetic return energy is plotted for a large number of different tunneling times t' in Figure 2.3.

It is sufficient to consider tunneling times $t' \in [0, T/2]$, because of the antisymmetry of the E-field. Electrons that appear in the continuum with $t' \in [T/4, T/2]$ return to the origin at some time $t > T/2$. The amount of kinetic energy that the electrons return with depends on the tunneling time, t'. In the middle plot of Figure 2.3, we find that:

$$E_k \leq 3.17U_p,$$

where:

$$U_p = \frac{q^2\lambda^2 I}{8\pi^2\epsilon_0 c^3 m}$$

is the average oscillating kinetic energy that the electron has in the IR-field [2] [3]. This is one of the key results from the classical treatment of the electron trajectories because it implies that the maximal photon energy is $I_p + 3.17U_p$, where I_p is the potential energy of the bound electron.

2.3 Numerical Approach

In the previous section, the analytical equations for the classical trajectories, generated by monochromatic laser fields, were calculated. In the next section, we will consider more general fields with temporal envelopes and two colors. We disregard all spatial effects, such as phase matching and spatial envelopes.

[2] U_p is also known as the ponderomotive energy

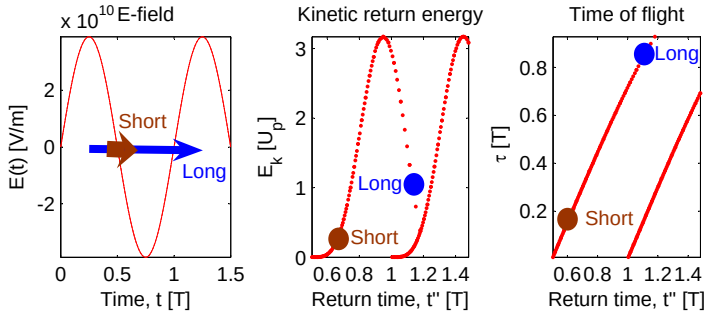

Figure 2.3: The left plot shows the IR field driving the harmonic generation. The blue arrow represents a long trajectory that tunnels at $t' \approx 0.25T$ (where the arrow starts) and returns approximately one period later, at $t'' \approx 1.25T$ (where the arrow ends). The longest returning trajectory spends one period in the continuum. Even longer trajectories must be considered if the the electron is not fully recombined when it returns to the atom. The red arrow represents a short trajectory that tunnels just before the electric field changes sign, $t' \approx 0.5T$, and then returns very quickly to the nucleus, $t'' \approx 0.5T$. The shortest trajectory possible spends no time in the continuum. The middle plot shows the kinetic energy that the electron can return with at different times. The right plot shows the corresponding time of flights, τ, i.e. the amount of time that the electron spends in the continuum before recombining with the atom. We define short trajectories to have $\tau < 0.65T$; and long trajectories to have $\tau > 0.65T$, see Figure 5.1 for more details.

Envelopes

It is possible, but cumbersome, to calculate the trajectories of particles in laser pulses. Instead of doing all this integrating, a MATLAB program is written that solves the classical trajectories numerically for arbitrary driving fields.

We choose to model the temporal envelope as a $\cos^2$-envelope, labeled Λ_N, and not as a Gaussian envelope, because a $\cos^2$-envelope becomes zero in a finite time. The Gaussian envelope, on the other hand, only approaches zero as the time goes to infinity, which complicates numerical calculations. The $\cos^2$-envelope is defined as:

$$\Lambda_N(t) = \cos^2(\omega t/2N) \times (\Theta(t + NT/2) - \Theta(t - NT/2)),$$

where N is the number of IR-periods that the envelope spans and the Θ's are step functions ensuring that the envelope is zero for $t \notin (-NT/2, NT/2)$. Multiplying the envelope with the carrier frequency gives the electric field of the laser pulse:

$$E(t) = E_0 \sin(\omega t + \phi_R) \times \Lambda_N(t),$$

where E_0 is the amplitude, ω is the carrier frequency and ϕ_R positions the oscillations relative to the envelope [3]. A typical laser pulse is found in the left plot of Figure 2.4.

When the harmonic generation is driven by a laser pulse, we find that the return energies are damped at the start and at end of the pulse. This is easy to understand because the driving field is weaker there, making the effective ponderomotive energy smaller.

The time of flight, τ, is independent of the applied intensity for continuous fields, which is easy to understand because the longest trajectory always spends one period, T, in the continuum before returning. There is, however, a small perturbation in the time of flight due to the slowly varying amplitude during each period of the pulse.

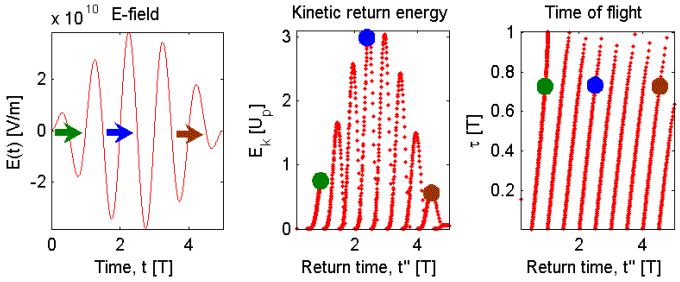

Figure 2.4: The arrows indicate trajectories that return with maximal kinetic energy. The early (green)- and the late (red) trajectories return with less energy than the center trajectory (blue), because the electric field is stronger in the center of the pulse.

[3] ϕ_R is sometimes called that Carrier-Envelope delay (C-E). Note that the C-E was defined for a sin-type E-field, and not for a cos-type E-field which might be a more common definition.

$\omega/2\omega$ Fields

We are especially interested in studying a bichromatic laser field, referred to as the $\omega/2\omega$ field. We add the second harmonic of the fundamental in the driving field:

$$E(t) = E_0(\sin(\omega t + \phi_R) + \xi \sin(2\omega t + \phi_B)),$$

where $\phi_R - \phi_B$ is the relative phase between the two laser beams and ξ is the relative amplitude. In experimental setups the 2ω field is usually generated using a phase matched doubling crystal. Continuous fields are easy to phase match because they consist of only one frequency. In HHG, on the other hand, all driving fields are short pulses which are hard to phase match because they have very broad bandwidths. Due to the poor phase matching of short pulses, the 2ω field is relatively weak, $\xi < 1$.

The middle plot of Figure 2.5 shows that the return energies of the electron will be different in consecutive half periods due to the 2ω field. Photons generated in consecutive half periods will therefore have different maximal energy, i.e. there will be two different cut off energies. In Figure 1.2 we experimentally observe these two cut offs. The two-cut-offs idea is semiclassical and we need the full quantum mechanical picture to verify it. This is done in later chapters using the Strong Field Approximation.

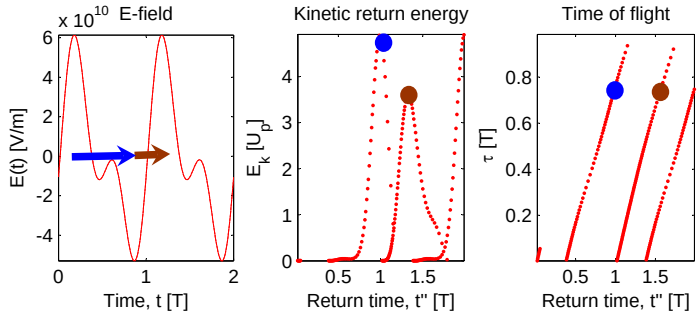

Figure 2.5: In the left plot we see that the $\omega/2\omega$ field is symmetric in T, rather than antisymmetric in $T/2$. In the middle plot, we see that the blue trajectories get higher kinetic return energies than the red trajectories. We associate the red trajectory with the low energy cut off and the blue trajectory with the high energy cut off.

2.4 Lagrangian Mechanics

Newton's second law is the quickest and easiest way to obtain the classical trajectories. There is, however, quite a large gap between these simple calculations and the quantum mechanical formulation of harmonic generation. This gap can be reduced using Hamiltonian mechanics and electromagnetic gauge transformations, obtained through Lagrangian mechanics [11].

In Lagrangian mechanics, potentials are used instead of forces. A charged particle in an electromagnetic field is expressed by the following Lagrangian:

$$L = L(t, \vec{r}, \vec{v}) = \frac{m}{2}\vec{v}^2 - q\Phi(t, \vec{r}) + q\vec{v} \cdot \vec{A}(t, \vec{r}),$$

where $\vec{r} = \vec{r}(t)$ is the position, $\vec{v} = \vec{v}(t) = \frac{d\vec{r}}{dt}$ is the velocity, q is the charge and m is the mass of the particle. Φ is the scalar- and $\vec{A}$ is the vector potential describing the EM-field [11]:

$$\begin{cases} \vec{E} &= -\nabla\Phi - \frac{\partial \vec{A}}{\partial t} \\ \vec{B} &= \nabla \times \vec{A}. \end{cases}$$

The action, S, plays an important role:

$$S = \int_{t',\vec{r}'}^{t,\vec{r}} dt'' L,$$

because the dynamics of the particle are obtained by finding paths, $\vec{r}(t)$ of stationary action. This is most often done with Euler-Lagrange's equation:

$$\delta S = 0 \Leftrightarrow \frac{d}{dt}\frac{\partial L}{\partial v_i} = \frac{\partial L}{x_i}.$$

Going ahead and solving for the classical trajectories is straightforward but it would be a waste of time, because the solutions were found in the previous section by other means. Instead, the next step is to obtain the Hamiltonian.

2.5 Hamiltonian Mechanics

While the Lagrangian is a function of time, position and velocity. The Hamiltonian is a function of time, position and canonical momentum, $\vec{p}$. The canonical momentum is defined though the Lagrangian as:

$$p_i = \frac{\partial L}{\partial v_i} = mv_i + qA_i,$$

and it is not the same as the kinetic momentum, $\vec{\Pi} = m\vec{v}$. In general, there is no physical interpretation of the canonical momentum because it is not gauge invariant [12]. This particular canonical momentum is a conserved quantity:

$$\dot{p} = m\ddot{x} + q\dot{A} = m\ddot{x} - qE = 0,$$

which we interpret as the drift momentum, corresponding to the net drift discussed earlier. The Hamiltonian of a particle in an EM-field is constructed from the Lagrangian using a Legendre transformation:

$$H = H(t, \vec{r}, \vec{p}) = \vec{p} \cdot \vec{v} - L = \frac{m}{2}v^2 + q\Phi = \frac{1}{2m}(\vec{p} - q\vec{A})^2 + q\Phi.$$

This Hamiltonian is the starting point of most undergraduate textbooks on quantum mechanics. This formulation of the problem is written in the Velocity gauge [4], which implies that the vector potential satisfies:

$$\nabla \cdot \vec{A}_v = 0.$$

[4] Also known as the the Coulomb gauge and the Transversality condition [13].

All relevant physical measurements are gauge invariant. Nonphysical quantities can be gauge dependent, see Table 2.1 for details.

QUANTITY	$\vec{r}$	$\vec{v}$	$\vec{\Pi}$	$\vec{p}$	$\vec{E}$	$\vec{B}$	Φ	$\vec{A}$
GAUGE INVARIANT	Yes	Yes	Yes	No	Yes	Yes	No	No

Table 2.1: Physical quantities are measurable and they must therefore be gauge invariant. The constructed quantities do not have to be gauge invariant because they are unmeasurable.

From electromagnetic theory it is known that the allowed gauge transformations are given by [1]:

$$\begin{cases} \Phi & \xrightarrow{\chi} & \Phi' - \frac{\partial \chi}{\partial t} \\ \vec{A} & \xrightarrow{\chi} & \vec{A}' + \nabla\chi, \end{cases}$$

where $\chi = \chi(t, \vec{r})$ is a scalar function. Changing the gauge from Velocity to Length is done using a particular χ_l:

$$\chi_l = -\vec{r}\cdot\vec{A}_v(t,\vec{0}) \rightarrow \begin{cases} \frac{\partial \chi_l}{\partial t} &= -\vec{r}\cdot\frac{\partial \vec{A}_v}{\partial t} = \vec{r}\cdot\left(\vec{E}(t,\vec{0}) + \nabla\Phi(t,\vec{0})\right) \\ \nabla\chi_l &= \nabla\left(-\vec{r}\cdot\vec{A}_v(t,\vec{0})\right) = -\vec{A}_v(t,\vec{0}). \end{cases}$$

Substituting the new potentials into the Hamiltonian yields:

$$H_l = \frac{1}{2m}\left(\vec{p} - q(\vec{A}_v - \vec{A}_v(t,0))\right)^2 + q\left(\Phi - \vec{r}\cdot(\vec{E}(t,\vec{0}) - \nabla\Phi(t,\vec{0}))\right).$$

We make some more approximations: assuming that the particle is close to the origin at all times $\vec{A} \approx \vec{A}(t,\vec{0})$; and that the external field is a slow function of position: $\nabla\Phi \approx 0$ which finally yields:

$$H_l = \frac{1}{2m}p^2 - q\vec{r}\cdot\vec{E},$$

where the scalar potential has been chosen so that $\Phi(t,\vec{0}) = 0$. This Hamiltonian is the starting point for the Strong Field Approximation that will be used in the quantum mechanical treatment of high order harmonic generation in a later chapter. In the Length gauge and within these approximations, the canonical- and the kinetic momentum are identical. This makes the final expression look very intuitive; the Hamiltonian is simply the sum of the kinetic- and the potential energy:

$$H = E_k + V = mv^2/2 - qxE,$$

in the one dimensional case.

It is worth stressing that the conclusions obtained in this classical treatment are very useful for understanding the process of harmonic generation. The Simple Man's Model and the Cut Off Law provide great insight and physical intuition, which must be appreciated before the level of abstraction can be increased. The derivation of the Hamiltonian and the distinction between different kinds of momenta, might be harder to appreciate at first, but they are absolutely necessary for understanding the full quantum mechanical treatment of the process.

Chapter 3

Quantum Interference

3.1 Limitations of the Classical Theory

When an atom interacts with a strong laser field, an electron can tunnel out though the atomic potential and gain a large kinetic energy in the continuum. The laser field then changes sign and the electron is pulled back to the atom with a kinetic energy ranging continuously between:

$$0 < E_k(t'') < 3.17U_p,$$

where t'' is the return time and U_p is the average oscillating kinetic energy of the electron in the laser field. Combining the kinetic return energy with the ionization potential of the atom, I_p, yields the *cut off* law: Photons that can be produced in HHG have energies, E_γ, ranging between:

$$0 < E_\gamma < 3.17U_p + I_p,$$

depending on whether the electron is fully recombined or simply decelerated by the atom [3]. When studying the experimental spectrum in Figure 1.2, we can verify that the cut off law is valid. We also observe that the emitted photons are not continuously distributed. For the IR field, the emitted HHG photons come in discrete peaks centered at the odd harmonics:

$$E_{\gamma_{IR}} = \hbar\omega H_{odd},\ H_{odd} \in [1, 3, 5..., H_{CO}],$$

where H_{CO} is the cut off harmonic and $\hbar\omega$ is the energy of the fundamental laser photon. The $\omega/2\omega$ field HHG photons are emitted at all harmonics:

$$E_{\gamma_{\omega/2\omega}} = \hbar\omega H_{all},\ H_{all} \in [1, 2, 3..., H_{CO}].$$

The *plateau* region, $5\hbar\omega < E_\gamma < \hbar\omega H_{CO}$, has roughly constant harmonic intensities; while the cut off region, $E_\gamma > \hbar\omega H_{CO}$, has strongly decreasing harmonic intensities. The lowest harmonics, $0 < E_\gamma < 5\hbar\omega$, are typically much more intense than the plateau harmonics.

The electrons can return with a continuous energy E_k, but we only detect photons with discrete energies. The discretization of the photon energies occur because the electron motion is repeated in time. If the electron is pulled up

and down only once, then the photon spectrum will be continuous. These conclusions are straight forward but rather abstract and mathematical. We will instead attempt to describe the photon generation in a quantum mechanical context, with the Feynman Path Integral formalism. This will give us more insight and understanding of the physical process. Interference of light can be modeled with each photon having a complex oscillating phase spinning at a specific rate:

$$e^{i\omega_\gamma t},$$

determined by the photon energy $E_\gamma = \hbar\omega_\gamma$. In this treatment, we assume that the photons are infinite in extent and we consider an arbitrary position, say $x = 0$. If there are many photons with the same energy then we will detect some intensity only if the photons don't destructively interfere. This is of course very well known, and a common feature of standing waves in laser cavities for instance. If we assume that N photons all have the same complex amplitude at a given point in space, then the probability P of detecting such a photon is proportional to the complex square of the sum of all photon phases:

$$P(E_\gamma, t) \equiv |\mathcal{P}(E_\gamma, t)|^2 \propto \left| \sum_{n=1}^{N} e^{i(\omega_\gamma t + \phi_n)} \right|^2 ,$$

where ϕ_n is the relative phase of photon n at the given point in space and $\mathcal{P}$ is called the complex probability. We use the proportional-to sign to avoid writing the normalizing factors explicitly.

Quantum mechanics extends this concept so that complex phases can be associated with particles. These phases have a slightly more complicated nature, because they depend on how much of the particle energy is kinetic versus potential.

3.2 Feynman's Path Integral

The probability of a particle moving between two points in space-time is expressed with the following bracket [19]:

$$P(x : x' \to x'', t : t' \to t'') = |\langle x'', t''|\ x', t'\rangle|^2 .$$

The motion of an electron can be expressed as a sum of complex numbers in the Feynman path integral formalism:

$$\langle x'', t''|\ x', t'\rangle \propto \sum_S e^{iS/\hbar},$$

where the sum includes all possible space-time paths from (x', t') to (x'', t'') and S is the corresponding action of each path [14]. A path is defined as a sequence of positions $x(t)$, one for each time t. As an example we consider:

$$\begin{cases} x &= (..., x_n, x_{n+1}, x_{n+2}...) \\ t &= (..., n, n+1, n+2, ...) \times \Delta t \end{cases}$$

where the path is written for small discrete time steps of Δt. In reality, we must take the limit where $\Delta t \to 0$. A path constructed like this, with x_{n+1}

being independent of x_n, implies that the velocity can by discontinuous. Some paths may appear unphysical and resemble Brownian motion[1] while others will coincide with those of classical mechanics.

All complex numbers corresponding to all paths, no matter how strange, are added with the same amplitude, resulting in a final complex number with a certain amplitude and phase. The square of this amplitude is proportional to the probability of the electron moving from (x', t') to (x'', t''):

$$P(x : x' \to x'', t : t' \to t'') \propto \left| \sum_S e^{iS/\hbar} \right|^2 .$$

Using this formalism for solving standard QM-problems is not very convenient, because you are often not interested in a particle moving from here to there. Particles in confining potentials are spread out in space and it is very hard to calculate the evolution of complex fields (wave functions) using the Feynman formalism. In fact, for confining potentials it is easier to use the standard Schrödinger formulation.

In high order harmonic generation, on the other hand, some electrons (or some part of an electron) can tunnel away from the confining atomic potential and end up in the continuum. There is no confining potential in the continuum, so we expect no strange QM-behavior due to confinement. Instead we can expect that the laws of classical mechanics rule the dynamics, with some additional interferences and quantum diffusion! We know from classical mechanics that the path a particle follows is given by the stationary action $\delta S = 0$:

$$S_c = \int_{(x',t')}^{(x'',t'')} dt \left\{ L(x_c(t), v_c(t), t) \right\},$$

where $x_c(t)$ is the classical path (c is short for classical) which satisfies the initial conditions $x_c(t') = x'$ and $x_c(t'') = x''$. Because the action is stationary at S_c, other paths $x'(t)$ that are close to the classical path $x(t)$, will have roughly the same action:

$$S'_c \approx S_c, \;\; x'_c(t) \approx x_c(t),$$

and therefore also approximately the same complex phase. The contributions from S_c and S'_c constructively interfere resulting in a complex vector with a complex phase of the classical action and a big complex amplitude.

We now consider a strange path $x_s(t)$ (s is short for strange) that is far from the classical $x_c(t)$. We also consider a path $x'_s(t)$ which is close to $x_s(t)$. Paths that are not close to the classical solution will not constructively interfere because the action is not stationary, the phase always changes very fast:

$$S'_s \not\approx S_s, \;\; x'_s(t) \approx x_s(t),$$

even if $x'_s(t)$ is very close to $x_s(t)$ at all times. Adding contributions from many strange narrow paths therefore result to nothing. For a schematic picture of the classical and strange paths, see Figure 3.1.

[1] Brownian motion is another word of a random walk in discrete steps. We gladly skip the additional complications that develop in the math, when the step size goes to zero!

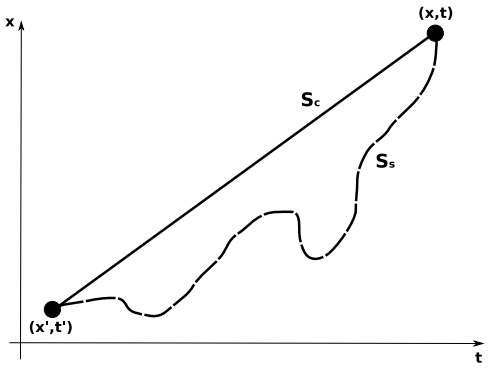

Figure 3.1: A free particle moves with constant velocity, i.e. along a straight line in space-time. This classical path is associated with a stationary action S_c. Another path, associated with the nonstationary action S_s, is unphysical in the classical sense but may contribute to results predicted by quantum mechanics. It is, however, more and more probable that the electron follows the classical path when the distance $\Delta x = |x' - x|$ increases.

We proceed by neglecting all strange paths and approximating the sum with a single contribution from the classical solution [2]. The sum is reduced to a single complex number:

$$\langle x'', t''|\ x', t'\rangle \propto e^{iS_c/\hbar},$$

where (x'', t'') must be somewhere along the classical path $x_c(t)$ connecting to the tunneling at (x', t'). If (x'', t'') is some other point, then the bracket is zero, resulting in zero probability of making the transition. We are therefore requiring that the electron moves on the classical trajectories, and that it has a complex phase which is given by the action in units of $\hbar$. The phase of the electron will be used to keep track of the phases of the generated photons in the high order harmonic generation.

Photon Creation and Interference in HHG

The next step is to consider the consequence of multiple tunneling times. There are many tunneling times t'_n that all result in classical trajectories returning to the atom with a specific kinetic energy $E_k \equiv E_k(t''_n)$, where n labels all possible contributions. We assume that the electron is fully recombined and that it generates photons with energy $E_\gamma = E_k + I_p$ when it returns at time $t''_n \equiv t''_n(t'_n)$. The tunneling probability depends on the instantaneous magnitude of the E-field, and there are also different probabilities for different scatterings, but we will not worry about these effects [3].

The probability of creating a photon with energy E_γ is proportional to the square of a sum of all the complex contributions from all electron trajectories

[2] This approximation works fairly well for the high HHG photons, $\hbar\omega H > I_p$; and not at all for the low HHG photons, $\hbar\omega H < I_p$.

[3] The dipole transitions from bound to the continuum is roughly constant for the electron energies considered here [15].

returning to the nucleus:

$$P(E_\gamma) \propto \left| \sum_n e^{i\phi_n(t)} \right|^2 ,$$

where $\phi_n(t)$ is the phase of photon n at time t.

We know that there are 4 trajectories per period that can contribute to a specific E_γ: 1 short and 1 long from each half period of the ω field [4].

HHG of Monochromatic Fields

We neglect the long trajectories and consider only the contributions from the short trajectories. We furthermore assume that the electron is fully recombined when it returns to the atom. We label the short trajectories with n. Figure 3.2 shows a schematic picture of the photons being created by two different short trajectories: n and $n+1$.

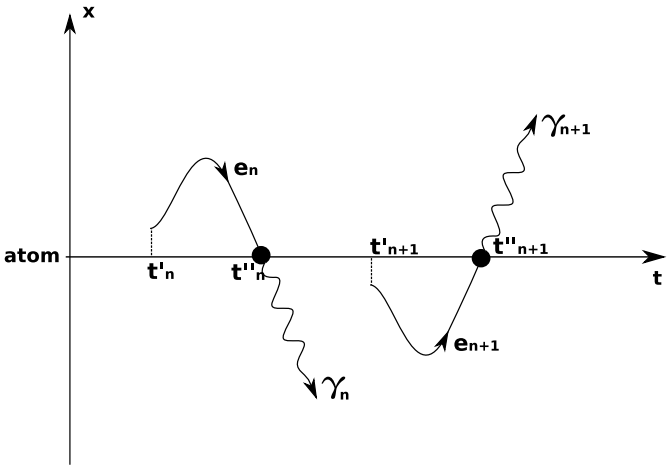

Figure 3.2: Photons with energy E_γ are produced by a large number of trajectories. There are two such trajectories per period, one which is created when the driving field is positive and another when the field is negative. In order to find out if there is a nonzero probability of detecting such a photon, we need to consider all generated photons γ_n and we need to keep track of all their individual phases.

We now determine the phase of a photon at time t generated at time t'' by an electron that tunneled at time t'. The phase is constructed by multiplying the complex numbers of four individual processes, see Table 3.1.

The recombination phase is inspired by the quantum mechanical bracket for dipole recombination:

$$\langle g| \, x \, |c\rangle ,$$

[4] If we had not already assumed that the electron is fully recombined at the atom, then we would also have contributions from even longer trajectories corresponding to electrons that were not fully recombined on their first rendez-vous with the atom.

PROCESS	Bound	$\rightarrow$	Continuum	$\rightarrow$	Recomb.	$\rightarrow$	Photon
PHASE	$e^{iI_p t'_n/\hbar}$	$\times$	$e^{i\pi n}e^{iS_n/\hbar}$	$\times$	$e^{-iI_p t''_n/\hbar}$	$\times$	$e^{iE_\gamma(t-t''_n)/\hbar}$

Table 3.1: The electron oscillates with the binding energy, $I_p/\hbar$, when it is bound to the atom. After tunneling, it accumulates a phase corresponding to the classical action of the trajectory in the continuum, $S_n/\hbar$. It then recombines and the generates a photon. The photon oscillates with the photon energy, $E_\gamma/\hbar$.

where $|c\rangle$ is a continuum state, $\langle g|$ is a ground state and x is the dipole operator along the linear polarization [13]. Note that the ground state phase is complex conjugated, which results in a total phase that depends on the difference between the phase of the electron that stays in the ground state and the phase of the returning electron. This fact has been used by P.B. Corkum to interpret the high order harmonic process as a beam splitter with interfering electrons wave functions [6]. We have inserted a factor $e^{i\pi n} = (-1)^n$ in the continuum phase to account for the changing sign of the E-field between each half period. For monochromatic, continuous fields we have:

$$\begin{cases} t'_n = t'_0 + nT/2 \\ t''_n = t'_n + \tau_n \\ \tau_n = \tau \\ S_n = S, \end{cases}$$

where n extends from minus- to plus infinity. Note that all S_n are equal, even for consecutive trajectories: n and $n+1$, which move in opposite directions.

All factors that do not depend on n can be neglected. We find that the probability of generating a photon with energy $E_\gamma \in [I_p, I_p + 3.2U_p]$ is proportional to:

$$P(E_\gamma) \propto \left| \sum_n e^{-i(E_\gamma T/2\hbar + \pi)n} \right|^2 .$$

The normalization factor ensures that the probability is nonzero only when the phases in the sum are constructive. The probable energies are therefore:

$$E_\gamma T/2\hbar + \pi = 2\pi Z,$$

where Z is an integer. Some rearranging result in odd harmonics of the fundamental $\omega = 2\pi/T$ frequency:

$$E_\gamma = \hbar\omega(2Z - 1),$$

which is the harmonic structure we expected to find. Note that we don't need to calculate the value of S_n to obtain this result. The probability function, $P(E_\gamma)$, should be seen as a toy model of HHG. It allows us to play with HHG and obtain qualitative quantum mechanical results that are very hard to derive from the full quantum mechanical treatment. In the next section we play with $P(E_\gamma)$ and figure out how the harmonics respond to a $\omega/2\omega$ driving field. The results are verified in the next chapter using the Strong Field Approximation.

Phase Perturbations from the 2ω Field

We modify $P(E_\gamma)$, so that it includes effects from the 2ω field, by inserting a small antisymmetric phase perturbation $e^{(-1)^n\delta}$:

$$P(E_\gamma) \propto \left| \sum_n e^{-i(E_\gamma T/2\hbar+\pi)n+(-1)^n\delta} \right|^2 .$$

The perturbation is periodic in T, and it can be used to describe the 2ω field as a perturbation on the IR field in the harmonic generation with $\omega/2\omega$ fields, see Figure 3.3. We interpret 2δ as the continuum action difference, $S_{n+1} - S_n$, of electrons from two consecutive half periods: n and $n+1$. It is not necessary to know the the analytical form of δ at this point.

Even Harmonics

Inserting even harmonics: $E_\gamma T/2\hbar = 2\pi Z$, where Z is an integer, into $P(E_\gamma)$ results in:

$$P(E_\gamma = 2Z\hbar\omega) \propto \left| \sum_n e^{-i(\pi n+(-1)^n\delta)} \right|^2 \propto |\sin\delta|^2 ,$$

because the probability is constructive along the imaginary axis. This is reasonable because the even harmonics must vanish for $\delta = 0$, i.e. when the driving field is monochromatic.

Odd Harmonics

Inserting odd harmonics: $E_\gamma T/2\hbar = \pi(2Z+1)$, where Z is an integer, into $P(E_\gamma)$ implies that:

$$P(E_\gamma = (2Z+1)\hbar\omega) \propto \left| \sum_n e^{-i(-1)^n\delta} \right|^2 \propto |\cos\delta|^2 .$$

It is reasonable to assume that neighboring harmonics have similar phase perturbations: $\delta_n \approx \delta_{n+1}$. We therefore conclude that the even and the odd harmonics behave in *opposite* ways when they are equally perturbed by $(-1)^n\delta$.

Analytical Derivation of δ

The $\omega/2\omega$ field can be modeled in terms of the vector potential:

$$A(t) = A_R(t) + A_B(t) = A_0\left(\cos(\omega t) + \xi_A\cos(2\omega t + \phi_B)\right),$$

where R is short for red (ω), and B is short for blue (2ω). The relative vector potential amplitude, ξ_A, is given by the relative electric field amplitude: $\xi_A = \frac{1}{2}\xi$, for continuous fields. The relative delay between the two fields is denoted ϕ_B.

It is tricky to find the analytical equation for δ in general $\omega/2\omega$ fields. The main problem is that the tunnel- and return times change between consecutive half periods for given return energies. It is, however, possible to find an approximate equation for δ when the 2ω field is very weak, if we assume that

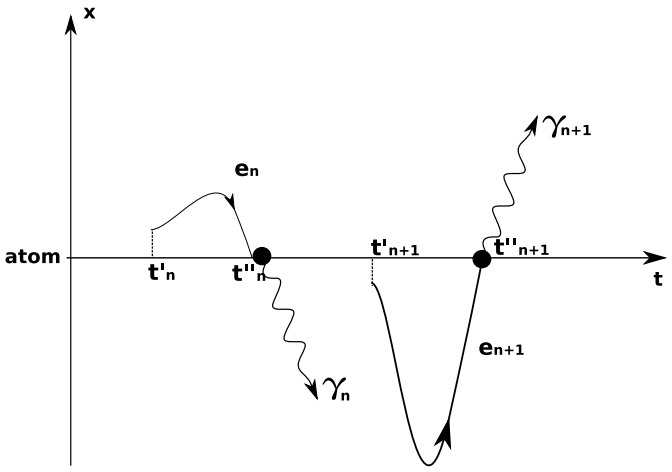

Figure 3.3: For antisymmetric perturbations, the electron trajectories with return energy E_k will be different depending on the sign of the electric field. There will be one slightly shorter (n) and one slightly longer trajectory ($n+1$). The photons can interfere because they have the same energy so wee need to consider their relative phases. We assume that the short trajectory accumulates less phase than the long trajectory: $S_n < S_{n+1}$. We include the phase difference by setting: $S_n = S_0 - \hbar\delta$ and $S_{n+1} = S_0 + \hbar\delta$, where it is not necessary that: $S_0 = S$.

the trajectories are not perturbed at all by the 2ω field [6]. The unperturbed velocity $v_R(t,t')$ from a monochromatic field, ω, is:

$$v_R \equiv v_R(t,t') = -\frac{qE_0}{m\omega}\cos(\omega t) + v_D(t'),$$

with the drift velocity $v_D(t') = \frac{qE_0}{m\omega}\cos(\omega t')$, where t' is the tunneling time. We can approximate the tunneling time t' as a linear function of the return time t'' for the short trajectories [5]:

$$t' \equiv t'(t'') = t'' - \tau(t'') \approx -0.44t'' + 0.72T.$$

We write the action of the electron in the $\omega/2\omega$ field as:

$$S = \int_{t'(t'')}^{t''} dt \left\{ \frac{mv_R^2}{2} + qv_R \times A_0 \left(\cos(\omega t) + \xi_A \cos(2\omega t + \phi_B)\right) \right\} \equiv ...$$

$$\equiv S_R(t'') + \hbar\delta(t''), \quad \delta(t'') = \frac{A_0\xi_A}{\hbar}\int_{t'(t'')}^{t''} dt \left\{ v_R \times \cos(2\omega t + \phi_B) \right\},$$

where $S_R(t'')$ is the action of an electron returning at time t'' from a short trajectory in the ω field. The second term, $\delta(t'')$, describes how much the electron phase is perturbed by the 2ω field. Evaluating the integral in δ is a simple task, using Euler's formula:

$$\delta(t'') = -\frac{q^2E_0^2\xi}{2\hbar m\omega^2}\int_{t'(t'')}^{t''} dt \left\{ (\cos(\omega t) - \cos(\omega t')) \times \cos(2\omega t + \phi_B) \right\} = ...$$

$$= -\frac{U_p}{\hbar\omega}\sqrt{\mathcal{R}_I}\left[\sin(\omega t + \phi_B) + \frac{1}{3}\sin(3\omega t + \phi_B) - \cos(\omega t')\sin(2\omega t + \phi_B) \right]_{t'}^{t''},$$

where we inserted the ponderomotive energy of the pure IR field, $U_p = q^2E_0^2/4m\omega^2$ and the relative intensity between the two beams, $\mathcal{R}_I = \xi^2$. We immediately see that δ has a simple sinusoidal dependence on ϕ_B. We rewrite δ and obtain an equation where this dependence can be seen more clearly:

$$\delta(\phi_B, t'') = -\frac{U_p}{\hbar\omega}\sqrt{\mathcal{R}_I}\,|C|\sin\left(\phi_B + \arg(C)\right),$$

where C is a complex number:

$$C = \left[e^{i\omega t} + \frac{1}{3}e^{i3\omega t} - \cos(\omega t')e^{i2\omega t} \right]_{t'}^{t''}.$$

The prefactor in the equation above is approximately:

$$-\frac{U_p}{\hbar\omega}\sqrt{\mathcal{R}_I} \approx 3.88 \times \sqrt{\mathcal{R}_I},$$

for $I = 1 \times 10^{18}$ W/m^2. In this regime, the phase perturbation will be small, $|\delta| < \pi/100$, when the relative intensity is less than 10%. We approximate the intensity of the even harmonics as:

$$I_{even} \propto |\sin\delta|^2 \approx |\delta|^2 \propto |\sin(\phi_B + \arg(C))|^2.$$

We now proceed and consider some specific trajectories:

[5] To do this, we use the fact that $\tau = 0,\ t'' = 0.5T$ for the shortest possible trajectory; and $\tau = 0.65T,\ t'' = 0.95T$ for the longest short trajectory. See the right plot in Figure 2.3, to verify that a linear approximation can be made to describe $\tau(t'') = t'' - t'$. This particular linearization works for electrons returning in the second half period: $t'' \in [0.5, 0.95]T$.

• **Photons with $E_\gamma \approx I_p$**

The shortest possible trajectory tunnels and returns at the same time: $t' = t'' = 0.5T$. Intuitively there can be no effect from the 2ω field because the electron spends no time in the continuum. In the equations, it is clear that there is no dependence on ϕ_B because $|C| = 0$ which makes $\delta = 0$.

• **Photons with $E_\gamma \approx I_p + 3.2U_p$**

Photons with energies in the cut off regime are created by the longest short trajectory: $t' = 0.3T,\ t'' = 0.95T$. We find that $\phi_B \approx 1.28 \pmod{\pi}$ rad makes the even intensity go to zero ($\delta = 0$) for $\mathcal{R}_I = 1\%$.

One Dominant Trajectory per Period

The tunneling probability depends on the instantaneous electric field strength in a nonlinear fashion. We have earlier explained that this leads to only one dominant trajectory per period for fields for certain $\omega/2\omega$ fields. The probability of generating a photon of energy E_γ is:

$$P(E_\gamma)_{one\ traj.} \propto \left| \sum_n e^{-in(E_\gamma)T/\hbar} \right|^2 ,$$

which is constructive for any harmonic: $E_\gamma = Z\hbar\omega$, with Z being an integer, which is exactly what we expect for a driving field that makes a permanent dislocation of the electron [6].

[6] There is a net displacement of the electron because the field only pulls the electron out in one direction.

Chapter 4

Strong Field Approximation

4.1 QM-Hamiltonian for HHG

This chapter closely follows Lewenstein's approximate method for solving the problem of high order harmonic generation using the Strong Field Approximation (SFA) [9] [16]. In the chapter on classical trajectories we derived the Hamiltonian in the Length gauge which is the starting point of this quantum mechanical treatment. We also found that the kinetic- and the canonical momentum were equal in this gauge within the dipole approximation:

$$\Pi \approx p.$$

In quantum wave mechanics we have:

$$p \equiv -i\hbar\nabla,$$

where $\nabla \equiv (\frac{\partial}{\partial x}, \frac{\partial}{\partial y}, \frac{\partial}{\partial z})$. The electron is initially bound to an atom, so we need to introduce an atomic potential $V(r) \propto -1/r$ into the Hamiltonian H:

$$H = \frac{\Pi^2}{2m} - qxE(t) + V(r),$$

where Π is the kinetic momentum operator, $qxE(t)$ is the electric dipole moment operator from a $\hat{x}$-linearly polarized IR-field $E(t)$ and $V(r)$ is the atomic potential [1]. The electron dynamics $|\Psi(t)\rangle$ from the Hamiltonian H are described by the time dependent Schrödinger equation:

$$i\hbar\frac{\partial}{\partial t}|\Psi(t)\rangle = \left[\frac{\Pi^2}{2m} - qxE(t) + V(r)\right]|\Psi(t)\rangle\,.$$

The equation above only describes the physics of one single electron. Atoms used in high order harmonic generation often have more than one electron, but we restrict the calculations to the Single Electron Approximation (SEA). It is reasonable that this approximation is valid, because once one electron has tunneled, the remaining electrons will be more strongly bound, making it less probable for them to tunnel. Different electrons do not interfere so most of the important features will be present in SAE and in Hydrogen like atoms.

[1] Inserting the $1/r$ term in the potential invalidates one of the assumptions we made in the classical chapter. The kinetic- and the canonical momentum will therefore differ in the vicinity of the atom, but this effect will be neglected, as explained in the assumptions section.

4.2 Assumptions

Solving for the electron dynamics is very hard. We therefore need to make three key assumptions, denoted I), II) and III), which allow us to make some useful approximations:

I) No internal resonances

The atom is described by one bound state only, denoted $|0\rangle$.
Resonant interactions between bound atomic states must be avoided. This implies that the ionization potential I_p must be much larger than the photon energy $\hbar\omega$ of the driving IR field:

$$I_p \gg \hbar\omega.$$

In the case of Argon and IR we have $I_p/\hbar\omega = 15.76/1.55 \approx 10$, which satisfies the requirement.

II) No depletion

The ionization is weak.
The IR-field intensity must be below the saturation intensity of the atom:

$$U_p < U_{sat}.$$

I_{sat} for Argon is 4×10^{14} W/cm^2, which therefore may not be exceeded. This implies that most of the electron population stays in the bound state at all times.

III) Free particle trajectories

The continuum electrons will not be influenced by the atomic potential $V(r)$.
For this to be valid, we need the ponderomotive energy to be larger than the ionization potential:

$$I_p < 2U_p,$$

so that the main acceleration of the electron is due to the IR-field, and not due to the atomic potential. For Argon, with $I_p = 15.76$ eV, the intensity therefore has to be at least 1.3×10^{14} W/cm^2.

4.3 Computational Basis

Before going into detail about the solution of the electron evolution, we need to discuss what basis to use in the quantum mechanical computation.

Bound State Basis

Using Assumption I), we replace all bound states with the ground state $|0\rangle$. The exact shape of this state is of little importance. For Argon it should be a p-state, but we will simplify things and assume that it is a s-state with full spherical symmetry. The ionization potential, $I_p = 15.76$ eV, is set to match that of Argon.

Continuum State Basis

The choice of basis for the continuum states is less trivial. First we consider the familiar momentum basis of a free particle [2]:

$$\varphi_{\Pi}(x) \equiv \langle x \,|\Pi\rangle = e^{i\Pi x/\hbar},$$

which is an eigenbasis of the kinetic energy operator:

$$-\frac{\hbar^2}{2m}\nabla^2 \,|\Pi\rangle = \frac{1}{2m}\Pi^2 \,|\Pi\rangle\,,$$

where Π^2 is an eigenvalue of the $-\hbar^2\nabla^2$ operator. When the electron is accelerated in the IR-field, the motion is given by the following bracket:

$$\langle\Pi|\, qx \,|\Pi'\rangle = iq\hbar\frac{\partial}{\partial\Pi}\delta(\Pi - \Pi'),$$

which follows from Fourier analysis [3]. Most readers are probably content with this basis in combination with Assumption III), but we need to stress that $|0\rangle$ and $|\Pi\rangle$ to *not* form an orthogonal basis.

We proceed by defining another momentum basis $\varphi_{\check{\pi}} \equiv \langle x \,|\check{\Pi}\rangle$ which includes the effect of the atomic potential:

$$\left[\frac{1}{2m}\Pi^2 + V\right]|\check{\Pi}\rangle = \check{\Pi}^2\,|\check{\Pi}\rangle\,,$$

where $\left[\frac{1}{2m}\Pi^2 + V\right]$ is an operator and $\check{\Pi}^2$ is the corresponding eigenvalue for the eigenvector $|\check{\Pi}\rangle$. The newly defined wavefunction, $\varphi_{\check{\Pi}}$, oscillates faster than φ_{Π} close to the atom because it is being accelerated to higher energies by the atomic potential, V. An orthogonal basis is obtained by combining $|0\rangle$ and $|\check{\Pi}\rangle$. This basis is great for symbolic computations even though we don't know the analytical shape of $\varphi_{\check{\Pi}}$.

Because $V \to 0$ for $|x| \to \infty$, we expect the two momentum functions to be equal far from the origin:

$$\varphi_{\check{\Pi}} \approx \varphi_{\Pi},\ |x| \gg 0.$$

This implies that: $x\varphi_{\Pi} \approx x\varphi_{\check{\Pi}}$, for any x. The electron dynamics in the continuum can therefore be approximated as independent of V:

$$\langle\check{\Pi}|\, qx \,|\check{\Pi}'\rangle \approx \langle\Pi|\, qx \,|\Pi'\rangle\,,$$

which essentially implements Assumption III).

[2] The following is written in one dimension, but the actual calculations must be carried out in three dimensions. See Bethe and Salpeter [17], page 36, for more details on the momentum basis expressed in spherical coordinates.

[3] The integral is taken over all space and it describes the transitions from one kinetic momentum state to the next, i.e. how the electron accelerates. In one dimension, we can evaluate the element in a more familiar notation by setting $x \propto t$ and $\Pi \propto \omega$:

$$F(te^{i\omega' t}) \propto \int dt\left\{te^{-i\omega' t}e^{i\omega t}\right\} \propto \frac{d}{d\omega}\delta(\omega - \omega'),$$

which is easy to verify using standard Fourier tables.

4.4 Electron State Expansion

The state of the electron is denoted as $|\Psi(t)\rangle \equiv |\Psi\rangle$. This state will include both bound- and continuum states and can be expanded in our orthogonal basis:

$$|\Psi\rangle = \left(a(t)\,|0\rangle + \int_0^\infty d^3\check{\Pi}\; b(\check{\Pi},t)\,\left|\check{\Pi}\right\rangle \right) e^{iI_p t/\hbar},$$

where the oscillation of the bound state has been factored out, making a real and slow. The left side of the Schrödinger equation is:

$$i\hbar\frac{\partial}{\partial t}\,|\Psi\rangle = i\hbar\left(\int d\check{\Pi}' \left\{ \dot{b}(\check{\Pi}',t)\left|\check{\Pi}'\right\rangle + ib(\check{\Pi}',t)I_p/\hbar\left|\check{\Pi}'\right\rangle \right\} + iI_p/\hbar\,|0\rangle \right) e^{iI_p t/\hbar}$$

where we set $a(t) \approx 1$ using Assumption II). The right side of the Schrödinger equation is:

$$H\,|\Psi\rangle = \left[\frac{\Pi^2}{2m} - qE(t)x + V\right]\left(|0\rangle + \int \check{\Pi}' b(\check{\Pi}',t)\left|\check{\Pi}'\right\rangle \right) e^{iI_p t/\hbar} = ...$$

$$= \left(\left[\frac{\check{\Pi}^2}{2m} - qE(t)x\right]|0\rangle + \int d\check{\Pi}' \left\{ \left[\frac{\check{\Pi}'^2}{2m} - qE(t)x\right] b(\check{\Pi}',t)\left|\check{\Pi}'\right\rangle \right\} \right) e^{iI_p t/\hbar},$$

where we hid the atomic potential using: $\left[\frac{\Pi^2}{2m} + V\right] = \frac{\check{\Pi}^2}{2m}$.

A differential equation for $b(\check{\Pi},t)$ is found by multiplying the Schrödinger equation from the left with $\left\langle\check{\Pi}''\right|$:

$$i\hbar\dot{b}(\check{\Pi}'',t) - I_p b(\check{\Pi}'') = ...$$

$$= b(\check{\Pi}'',t)\frac{\check{\Pi}''^2}{2m} - qE(t)\left\langle\check{\Pi}''\right| x\,|0\rangle + qE(t)\int d\check{\Pi}' \left\{ \left\langle\check{\Pi}''\right| x b(\check{\Pi}',t)\left|\check{\Pi}'\right\rangle \right\}.$$

The last term can be rewritten using Fourier analysis and a partial integration:

$$\hbar\frac{\partial b(\check{\Pi},t)}{\partial t} = -i\left(\frac{\check{\Pi}^2}{2m} + I_p\right) b(\check{\Pi},t) + iE(t)d_x^*(\Pi) + \hbar qE(t)\frac{\partial b(\check{\Pi},t)}{\partial\check{\Pi}_x}.$$

Note that the the field free transition element, $d(\Pi)$, from the ground state $|0\rangle$ to the continuum is computed using φ_Π rather than the unknown function $\varphi_{\check{\Pi}}$. This is a simplification that is made in SFA that is hard to justify. The element has been calculated by Lewenstein [4]:

$$d(\check{\Pi}) \overset{SFA}{\longrightarrow} d(\Pi) = \langle\Pi|\,x\,|0\rangle = i\frac{2^{7/2}\alpha^{5/4}}{\pi}\frac{\Pi}{(\Pi^2+\alpha)^3},$$

in atomic units, with $\alpha = 2mI_p$ in the case of hydrogen like atoms.

[4] A similar expression can be derived easily in the one dimensional case, where the transition element can be interpreted as the following Fourier transform:

$$F(te^{-a|t|}) \propto \int dt\left\{ te^{-a|x|}e^{i\omega t}\right\} \propto \frac{\omega}{(\omega^2+a^2)^2},$$

where $t \propto x$ and $\omega \propto \Pi$. Note the difference in power in the denominator.

The differential equation can be simplified using a clever trick. In the chapter on classical trajectories, we showed that the drift momentum, p_v, is a conserved quantity. We therefore make the following substitution: $b(\breve{\Pi}, t) \rightarrow \tilde{b}(p_v, t)$, where the kinetic momentum, $\breve{\Pi}$, was substituted for the drift momentum, $p_v = \breve{\Pi} + qA(t)$. The simplified differential equation becomes:

$$\hbar \frac{\partial \tilde{b}}{\partial t} = -i \left(\frac{1}{2m}(p - qA(t))^2 + I_p \right) \tilde{b} + iE(t)d(p - qA(t)),$$

which can be solved:

$$b(p_v, t) = i \int_0^t dt' \left\{ E(t')d_x(p_v - qA(t'))e^{-iS(p_v,t,t')/\hbar} \right\}.$$

The phase factor:

$$e^{-iS(p_v,t',t)/\hbar} = e^{-i\int_{t'}^t dt'' \left[(p_v - qA(t''))^2/2m + I_p\right]/\hbar} \equiv e^{-i\int_{t'}^t dt'' H(t'')/\hbar},$$

corresponds to the accumulated phase of the drift momentum state, which can be identified as the propagator operator of a time dependent Hamiltonian [19]. Note that we now use quantum mechanical states rather than the classical trajectories to describe the dynamics.

4.5 Dipole Emission

The electromagnetic radiation emitted from the atom is proportional to the atomic dipole $\langle x(t) \rangle$. We use the electron state $|\Psi(t)\rangle$ to calculate the expectation value of the electron position:

$$\langle x(t) \rangle \equiv \langle \Psi(t) | \, x \, | \Psi(t) \rangle \propto ...$$

$$i \int_{t_0}^t dt' \int d^3p_v E(t') d_x^*(p_v - qA(t)) d_x(p_v - qA(t')) e^{-iS(p_v,t,t')/\hbar} + c.c..$$

Interpretation:
(Reading the equation from right to left) The electron tunnels into the continuum at time t' with drift momentum p_v. It propagates in the continuum until it recombines to $|0\rangle$ at time t. The integral over drift momentum space accounts for all possible drift momenta.

The expression for $\langle x(t) \rangle$ can be simplified by approximating the integral over p_v using a mathematical technique, called the *saddle point approximation*. The action S is expanded in a 2^{nd} order Taylor series about the stationary points (the trajectories corresponding to classical mechanics). The approximated integral is a Gaussian which is easy to evaluate [5]. The dipole becomes:

$$\langle x(t) \rangle \propto i \int_{t-t_0}^t d\tau \zeta(\tau) d_x^*(p_s - qA(t)) e^{-iS(p_s,t,\tau)} E(t-\tau) d_x(p_s - qA(t-\tau)) + c.c.,$$

[5] There are some extra complications because the integrals are complex, but the idea is the same, see Ivanov's lecture for more details [18].

where p_s is the canonical momentum that corresponds to stationary action. We find p_s by requiring that the action S has a vanishing first derivative with respect to p_v:

$$\frac{\partial S}{\partial p_v} = \frac{\partial}{\partial p_v}\left(\int_{t-\tau}^{t} dt'' \left\{(p_v - qA(t''))^2/2m + I_p\right\}\right) = ...$$

$$\frac{\partial}{\partial p_v}\left(\tau p_v^2 - 2qp_v\int_{t-\tau}^{t} A(t'')dt'' + q^2\int_{t-\tau}^{t} A^2(t'')dt'' + 2m\tau I_p\right)/2m = ...$$

$$= \left(\tau p_v - q\int_{t-\tau}^{t} A(t'')dt''\right)/m = 0|_{p_v=p_s} \rightarrow\ p_s(t,\tau) = \frac{q}{\tau}\int_{t-\tau}^{t} A(t'')dt'',$$

where we used that the canonical momentum is conserved: $\dot{p}_v = 0$. The quantum diffusion is described by $\zeta(\tau)$:

$$\zeta(\tau) = \left(\frac{\pi}{\nu + i\tau/2m\hbar}\right)^{3/2},$$

which attenuates the amplitude of long trajectories, with big τ, making the recombination probability smaller [6].

4.6 Implementation

We approximate the dipole moment as a sum:

$$\langle x(t_m)\rangle \approx \sum_{n=n_0}^{m} \Delta x_{nm} \equiv i\Delta t \sum_{n=n_0}^{m} \zeta(\tau_{mn}) d_x^*(p_{mn} - qA(t_m))\times$$

$$e^{-iS(p_{mn},t_m,\tau_{mn})} E(t_m - \tau_{mn}) d_x(p_{mn} - qA(t_m - \tau_{mn})) + c.c.,$$

where the time is taken to be discrete $t_{n+1} = t_n + \Delta t$. The sum includes electron trajectories recombining at t_m which tunneled at $t_n \geq t_0$. The stationary drift momentum is approximated as a sum:

$$p_{mn} \equiv p_s(t_m, \tau_{mn}) \approx \frac{\Delta t}{\tau_{mn}} \sum_{i=n}^{m} qA(t_i),$$

which corresponds to an electron tunneling at t_n and recombining at t_m, spending a time $\tau_{mn} = t_m - t_n$ in the continuum.

It is clear that these approximations are not exact. There is, however, an easy way of verifying that the step size, Δt, is small enough for our purposes. Decreasing Δt, includes higher energies in the numerical calculation: Take the Fourier transform of the dipole moment, and verify that the entire plateau with some cut off is resolved. For intensities of 10^{18} W/m^2, we typically need 100 steps per period. More information about the implementation can be found in Appendix A.

[6] ν is a regulation constant from the integration.

Chapter 5

Calculations

5.1 Separation of Quantum Orbits

Most of our understanding of HHG comes from the classical trajectories. In the following section different types of classical trajectories (quantum orbits) are separated in the SFA formalism. This is done by limiting the integration bounds in the SFA equation for the dipole moment $\langle x(t) \rangle$, calculated in the previous chapter.

Separation of the Short Trajectory

The short trajectory includes all classical trajectories returning before the maximum kinetic return energy. In Figure 5.1, we find that this corresponds to trajectories that spend: $\tau < 0.65T$, in the continuum, where τ is the time of flight and T is the IR-period. Using the SFA we can therefore calculate the

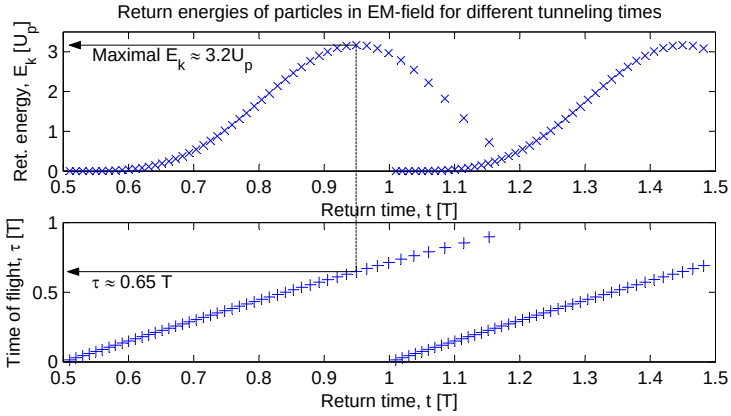

Figure 5.1: The maximal time of flight $\tau = 0.65$ for a short trajectory has the highest possible kinetic return energy $E_k = 3.2U_p$.

dipole moment from the short trajectory by limiting the lower bound in the

integration:

$$\langle qx(t)\rangle_{short} \approx i \int_{t-0.65T}^{t} d\tau \{...\} + c.c..$$

This is very useful because it allows us to separate the short trajectory contributions to the harmonic spectrum. In experiments, this separation can be done spatially [6]. Selection of the short trajectory is often done automatically due to phase matching effects [5]. We verify that the separation works, see Figure 5.2, where the intensity of the 35^{th} harmonic is plotted for increasing intensity. We conclude that the separation works well because there should be no interference in the harmonic emission as a function of intensity, if the harmonic is constructed by a single trajectory.

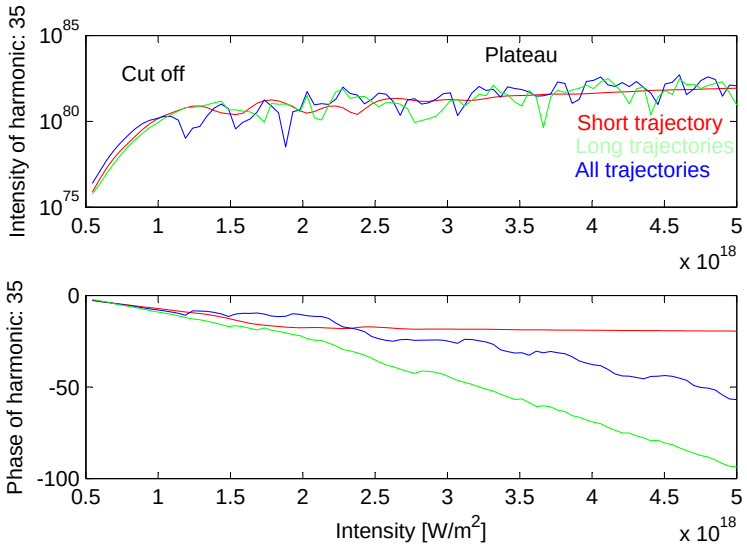

Figure 5.2: The intensity of a harmonic changes irregularly when the intensity is increased (blue line). This is due to an interference effect between the long and short trajectories. The long trajectories gain more phase than the short trajectory because they spend a longer time in the continuum. The interference pattern disappears when the short trajectory has been separated (red line) and the intensity is high enough ($I > 2.75 \times 10^{18}$ W/m^2). There is some interference close to the cut off for the short trajectories because the short and the long trajectories merge when $\tau \approx 0.65T$. In the lower plot we see that the phase of the short trajectory varies much slower than for the long trajectories. It is common to write the phase as $e^{-i\alpha I}$, which is possible due to the nice linear behaviour of the phase with intensity I in the plateau (from $I > 1.75 \times 10^{18}$ W/m^2). In this plot the green line includes more than one long trajectory and it is therefore irregular. We can, however, see that the first part of the plateau only includes one long trajectory because the green line remains smooth for higher intensities than the blue line.

Separation of the Long Trajectories

A similar separation for the first long trajectory is made by changing the integration bounds to:

$$\langle qx(t)\rangle_{long} \approx i\int_{t-T}^{t-0.65T} d\tau \{...\} + c.c.,$$

because this trajectory has $0.65T < \tau < T$. We can also study all long trajectories by setting:

$$\langle qx(t)\rangle_{all\ long} \approx i\int_{-\infty}^{t-0.65T} d\tau \{...\} + c.c..$$

This includes both the first long trajectory and trajectories that don't recombine on their first return to the atom. Quantum diffusion and rescattering, however, limit the contributions from the longer trajectories and it is therefore not necessary to integrate from minus infinity to obtain realistic results. In this Thesis integration from a few periods back was used to approximate the minus infinity. This includes the first few long trajectories.

Separation of Trajectories in Perturbed IR fields

The method described above assumes a continuous IR field. It will remain accurate also for small perturbations, such as a weak additional 2ω field. The separation is not exact for short pulses because the separation assumes continuous fields. We know, however, that the time of flight of continuous fields is intensity independent, so the we can expect the separation to work well for slowly varying pulses.

5.2 Many Cycle Fields

When the driving pulses are several tens of femtoseconds, we can model them as continuous fields. This is convenient because it reduces the required computational power and allows us to calculate harmonic spectra using SFA efficiently and fast.

In this Thesis, we use the word pulse for the driving field (10-30 fs) and the word (atto)burst for the generated emissions (100-300 as)

IR-field

The intensity emitted from HHG with a continuous IR field gives one attosecond burst per relevant trajectory [20]. In Figure 5.3 we can clearly see three bursts, corresponding to the short and two long trajectories.

$\omega/2\omega$-fields

When the 2ω laser is introduced, we can vary the relative delay- and the relative intensity of the pulses. Using the short trajectory filter, we find that most relative delays generate only one pulse per period, see Figure 5.4. This has been demonstrated experimentally by J. Mauritsson and co-workers [5].

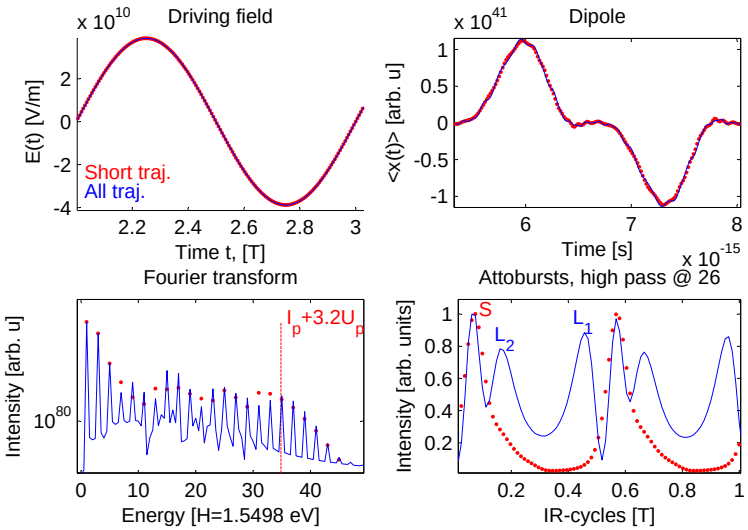

Figure 5.3: The top left plot shows the driving electric field and the top right plot shows the corresponding atomic dipole moment. The bottom left plot shows the harmonic spectrum. We verify that the cut off agrees with: $I_p + 3.2U_p$, from the classical treatment. The bottom right plot shows the temporal emission from the atom. There are three bursts per half period, one burst per trajectory type: The short (S), the long (L_1) and an even longer (L_2). L_2 is generated by electrons that originally were on a short trajectory but didn't recombine until on their second return to the atom ($\tau > T$). Even longer trajectories have been separated out. We identify the short trajectory using the short filter (red dots).

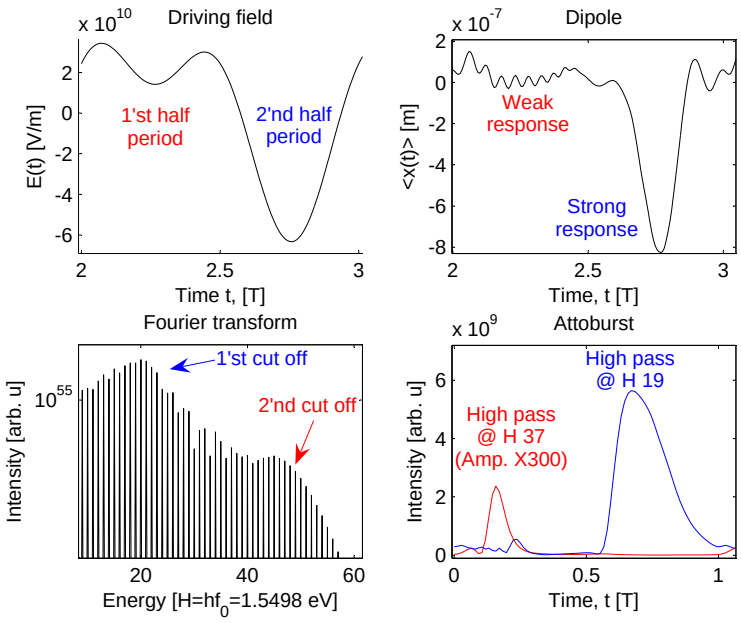

Figure 5.4: The $\omega/2\omega$ driving field can be used generate one attosecond burst per period. This is done by selecting the short trajectories; and synchronizing the beams so that the electric field in one half period is decreased (red) while it is increased in the other (blue). The dipole is clearly more excited in the 2^{nd} half period (blue) where the electric field is stronger. The spectrum can has two plateaus and two cut offs: one with high intensity and low electron energies (1^{st} cut off); and one with low intensity and high electron energies (2^{nd} cut off). Strong bursts are generated when the electric field is strong (blue) because the instantaneous ionization is larger, but the kinetic energy that the electrons can return with is small because the field that pulls them back is weak (red).

In the chapter on quantum interference, we argued, that the 2ω field can be described as antisymmetric perturbations $(-1)^n\delta$ in the phase between trajectories from different half periods in the IR field. This phase difference occurs because one of the trajectories gets longer, and the other gets shorter. The result of this perturbation is a sinusoidal oscillation in the harmonics:

$$\begin{cases} I_{even} \propto |\sin\delta|^2 \\ I_{odd} \propto |\cos\delta|^2. \end{cases} .$$

Increasing the relative intensity of the 2ω field, increases δ in a nonlinear fashion, and reveals the predicted oscillations, see Figure 5.5.

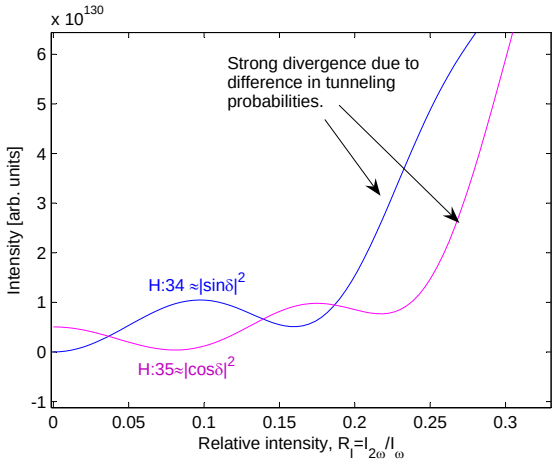

Figure 5.5: Increasing the relative intensity, $\mathcal{R}_I$, of the 2ω field gradually increases δ between the contributing trajectories in each harmonic. For harmonic 34 and 35, there are some nice sinusiodal oscillations before the harmonics diverge. The divergence is due to the tunneling probabilities changing, making one trajectory per period dominant.

Very Weak Perturbing 2ω-field

When the 2ω field is very weak, the antisymmetric perturbations are very small, $|\delta| \ll 1$:

$$\begin{cases} I_{even} \propto |\sin\delta|^2 \approx |\delta|^2 \\ I_{odd} \propto |\cos\delta|^2 \approx 1, \end{cases} .$$

Figure 5.6 shows that a 2ω field, with 0.1% relative intensity, perturbs the harmonic structure in the predicted fashion. In a previous chapter we computed that δ is a simple function of the relative phase; and a complicated function of the harmonic energies. We verify that the harmonics oscillate with ϕ_B as predicted: $\delta \approx |\sin(\phi_B + \arg(C))|^2$. We note that the oscillation off-set, $\arg(C)$, becomes constant in the cut off and that the even harmonics have zero intensity for $\phi_B \approx 1$ rad. This is quite close to 1 rad which was computed in the previous chapter.

In this regime, Corkum and co-workers have made in situ measurements of the harmonic phases. They obtain an analytical expression for δ by assuming that the trajectories are unchanged but that the action is slightly perturbed due to the 2ω field [6]. We verify that the in situ method gives the same result as the well known RABBITT technique, see Figure 5.7.

Weak Perturbing 2ω-field

When the intensity of the perturbation is increased to 1% of the IR, the phase difference becomes larger $|\delta| < \pi/2$ and the odd harmonics start to decrease in intensity:

$$\begin{cases} I_{even} \propto |\sin\delta|^2 \approx |\delta|^2 \\ I_{odd} \propto |\cos\delta|^2 \approx |1-\delta^2/2|^2. \end{cases}$$

When the phase difference becomes large enough ($\delta > \arctan(1) \approx 0.79$) the even harmonics will become more intense than the odd harmonics for some delays, this can be seen in Figure 5.8.

In this regime we can also control the emission time of the long trajectory as seen in Figure 5.9. The short trajectory, on the other hand, is mostly unaffected by the relative phase because it spends such a short time in the continuum.

Intermediate Pertubing 2ω-field

A tunable axis starts to form. Small additional contructive peaks appear in the spectrum as side bands to a main tunable axis due to δ exceeding π, see Figure 5.10.

Strong Perturbing 2ω-field

When the perturbing 2ω fields gets even stronger, 40% of the IR intensity, the tunneling probablities play an important role. One short trajectory per period becomes dominant creating a harmonic spectrum with a tunable peak in the plateau, $0 < \phi_B < 2$ rad. The tunable axis indicates that the generated bursts can be tuned to any central frequency in the cut off. At the end of the chapter on quantum interference, we showed that single bursts are obtained when the even and the odd harmonics are of equal strength. We therefore expect the tunable axis to generate one burst per period. The single burst generation energy can be fine tuned from the ionization potential to the cut off, see Figure 5.11. The remaining part of the spectrum, $2 < \phi_B < \pi$, contains two attobursts with comparable intensity per period. This results in a pattern that resembles the case of weak-intermediate relative intensities. These is a side band structure in the spectrum next to the tunable axis. The side bands can be reproduced qualitatively using the approximate equation for δ, calculated in the last part of the chapter on quantum interference [1].

Being able to amplify specific parts of the harmonic spectrum is useful, because it enables us to create attobursts with specific energies. These bursts can be used to make precise experiments on electron states in atoms and molecules.

[1] Note that the approximate δ is not valid in this regime of $\omega/2\omega$ fields and that even higher relative intensities have to be applied in the equation to obtain side band structures.

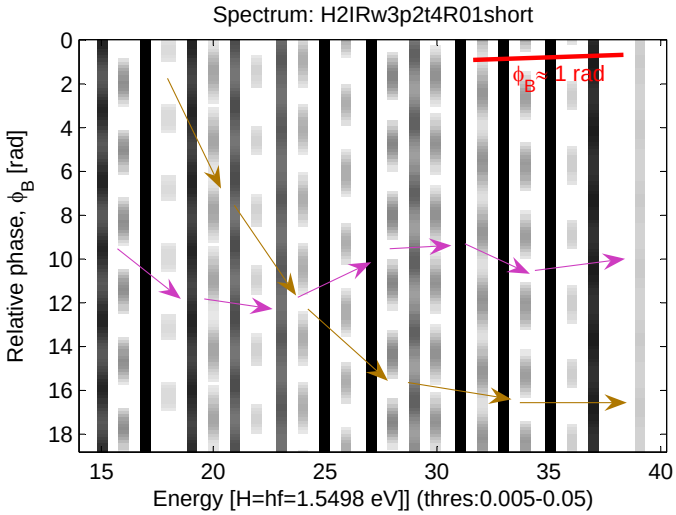

Figure 5.6: For perturbations of 0.1% relative intensity, the odd harmonics remain dominant (solid dark lines). The even harmonics can be controlled by adjusting the relative delay between the two fields. At the high harmonics (H:32-38), δ becomes almost constant (or shifted by integer values of π between the even harmonics). In the plateau ($H < 30$), δ changes smoothly from harmonic to harmonic. Two paths of arrows have been hand drawn on the spectrum indicating the difficulty of knowing how the phase changes.

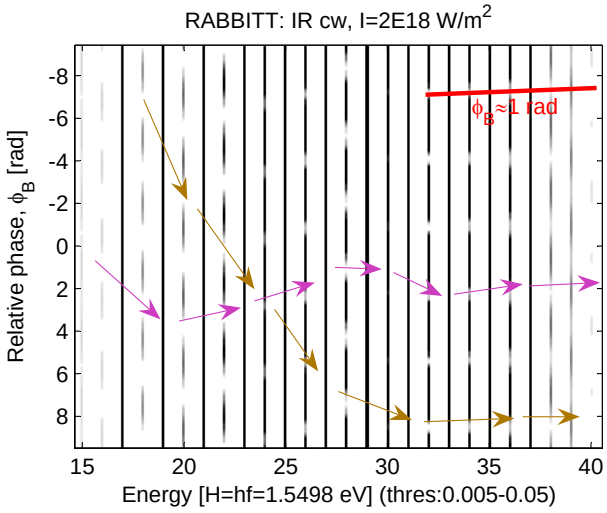

Figure 5.7: The harmonic phases can be determined using the RABBITT technique. The pattern is essentially the same for the two methods, which validates the in situ measurement. The same paths of arrows have been hand drawn to ease the comparison between the two spectra.

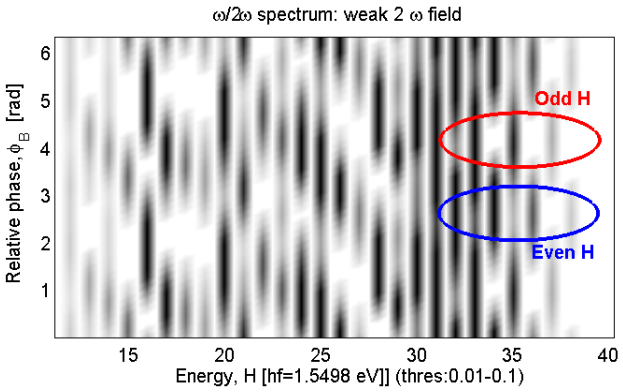

Figure 5.8: For perturbations with 1% relative intensity, both even and odd harmonics depend on the relative delay between the laser beams. In the high harmonics (H:31-38) we can amplify either the odd (red) or the even (blue) harmonics. The oscillation offset, $\arg(C)$, is constant in this region. In the plateau ($H < 30$), δ changes smoothly and fast.

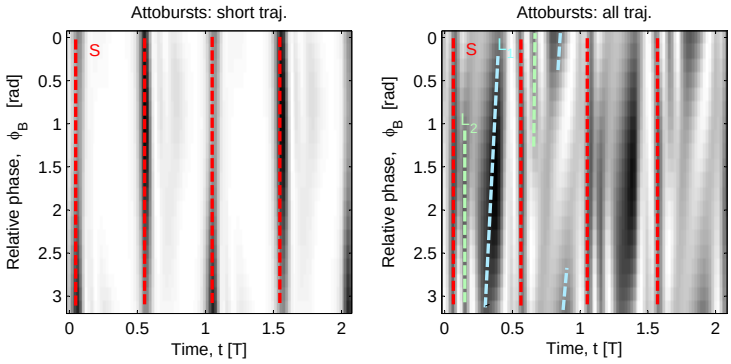

Figure 5.9: The left plot shows attobursts from the short trajectories (S). The right plot shows the attobursts from all trajectories, including the short (S), the long (L_1) and an even longer (L_2). The emission of the attosecond burst from the long trajectory can be controlled by adjusting the relative delay between the IR and the 2ω beam. The other two bursts are mostly unaffected by the relative delay: The short because it is only in the continuum for a short time; and the longer because it is in the continuum for nearly a whole period.

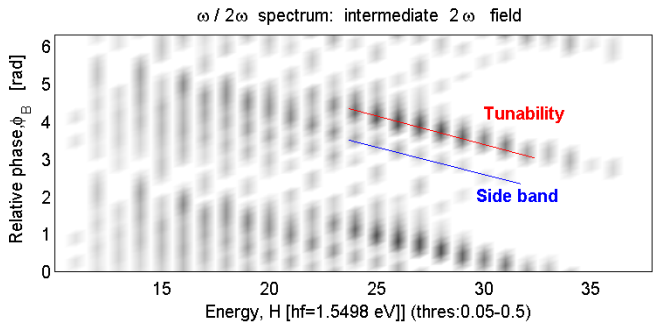

Figure 5.10: When the 2ω field has an relative amplitude of 20%, the harmonic spectrum looks complicated because δ exceeds π for some relative delays between the laser beams. We also begin to see a tendency of the harmonics to line up along a tunable axis (red). This structure becomes more visible for even higher relative intensities.

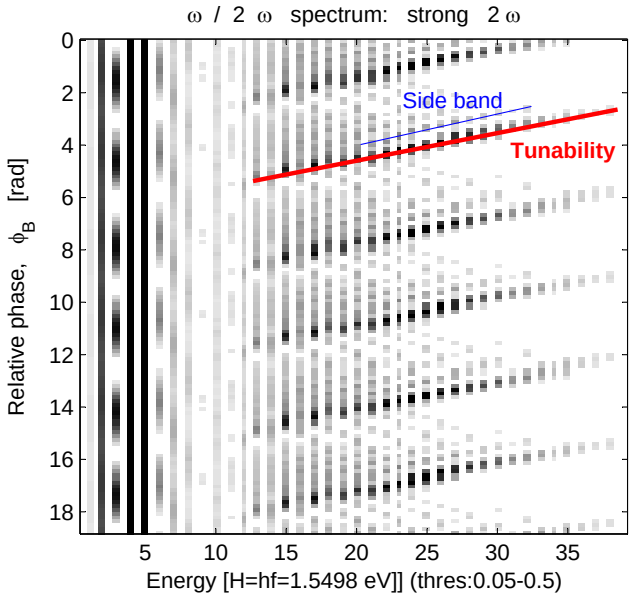

Figure 5.11: When the perturbing 2ω field is strong, 40% relative intensity, the relative delay between the laser beams can be tuned so that a specific part of the spectrum is amplified (red line). In this way, attobursts can be generated with fine tuned energies. Close to the tunability axis, there are some side bands.

5.3 Single Attosecond Bursts

We will now turn our attention to short driving pulses (FWHM < 12 fs) and investigate the possibility to create an isolated attosecond burst per driving pulse. Making the driving pulse short reduces the number of bursts because the E-field at the edges of the pulse is not strong enough to generate harmonics. We define a single attosecond burst as a sequence of bursts where the second strongest burst is less than 10% of the strongest burst.

There are many potential applications for single attosecond bursts. Making the driving pulse very short is a brute force approach of generating such bursts. Reducing the laser pulse to the critical duration from 10 fs to 5 fs can be done by broadening the spectrum using filament or capillary methods, but these methods are hard to engineer. It is therefore of great interest to generate single bursts with a more sophisticated technique. We investigate the possibility of creating single attosecond bursts using a combination of slighly longer driving IR pulses and 2ω pulses. Recent experiments with unlocked phase and single shots have been carried out by Y. Oishi [8]; and with locked phase by E. Gustafsson.

IR-pulses

It has been shown by A. Baltuska that single attosecond bursts can be created from 5 fs IR laser pulses [7]. In this Thesis, simulations have been made to verify that the maximal IR duration of the driving pulse is somewhere between 4 and 5 fs (FWHM) for single attoburst generation. The driving IR pulses are modelled in terms of the vector potential:

$$A(t) = A_0 \cos(\omega t + \phi_R) \times \Lambda_N(t),$$

where ϕ_R is carrier-evelope (C-E) phase and $\Lambda_N(t)$ is a N period long $\cos^2$-envelope centered at $t = 0$. The advantage of writing the electric field in terms of the vector potential is that it reduces the number of numerical integrations that have to be carried out in the SFA calculation. The disadvantage is that the laser pulse will get slighly distorted for very short envelopes (N small). This effect occurs because:

$$E(t) = -\frac{dA}{dt} = A_0 \left(\omega \sin(\omega t + \phi_R) \times \Lambda_N - \cos(\omega t + \phi_R) \times \frac{d\Lambda_N}{dt} \right),$$

where the first term is the correct shape for the electric field; and the second term is an error term. We note that the error term vanishes for large N because the error depends on $1/N$:

$$\frac{d\Lambda_N}{dt} = \frac{d}{dt} \left\{ \cos^2 \left(\frac{\omega}{2N} t \right) \right\} = ...$$

$$= -2 \cos \left(\frac{\omega}{2N} t \right) \sin \left(\frac{\omega}{2N} t \right) \times \frac{\omega}{2N}, \; t \in [-TN/2, TN/2].$$

In the following, we will study pulses with $N = 4$, which is quite critical, becuase the error term has an amplitude of 25% [2].

In total, we have a 4 dimensional parameter space:

[2] The program has not been verified to be accurate for short driving pulses.

Envelope duration	N
IR intensity	I
C-E delay	ϕ_R
High pass filter	H_{hp}

A high pass filter needs to be applied to select the single attosecond bursts. In the calculations, this filter is modelled as a discrete stepfunction that removes all contributions from all frequencies below a specific harmonic H_{hp}.

We study pulses with $N = 4$, which corresponds to approximately 4 fs (FWHM), and with intensities from 1×10^{14} - to 2×10^{14} W/cm^2 . Changing the C-E phase dramatically alters the cut off structure and the number of bursts produced, see Figure 5.12.

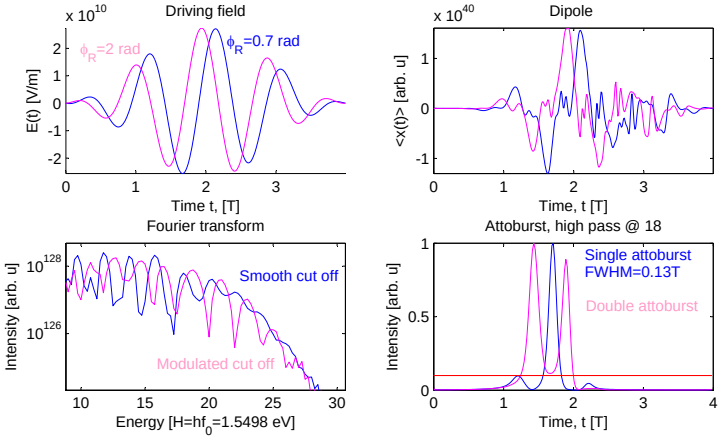

Figure 5.12: Single attobursts are produced for a specific C-E delay, $\phi_R = 0.7$ (blue line). The cut off is smooth because of there is only one trajectory contributing to the burst. Changing the C-E delay, to $\phi_R = 2$, results in two attobursts and a modulated cut off.

Single attosecond bursts can be identified in the spectrum as nonmodulated regions. The modulation is a result of several electron trajectories generating photons that interfere at the same energies. We find that single attosecond pulses can be produced with a high pass filter at harmonic $H_{hp} = 27$ for a specific C-E delay:

$$\phi_R \approx 0.8 \pm 0.1 \text{ rad},$$

which approximately corresponds to a cos type driving field. The high pass filter is set as low as possible, without allowing multiple bursts, in order to keep as much of the spectrum as possible. A broad bandwidth implies possibility of short pulses, and a low setting on the high pass filter also implies a larger number of photons (high conversion efficiency). The calculations are made with the short filter, there are therefore no bursts from the long trajectories.

The C-E phase determines the harmonic structure in the plateau, see Figure 5.13. With $I = 1 \times 10^{14}$ W/cm^2 we can move harmonics from odd to even by

simply changing the C-E phase (works only for few cycle driving pulses).

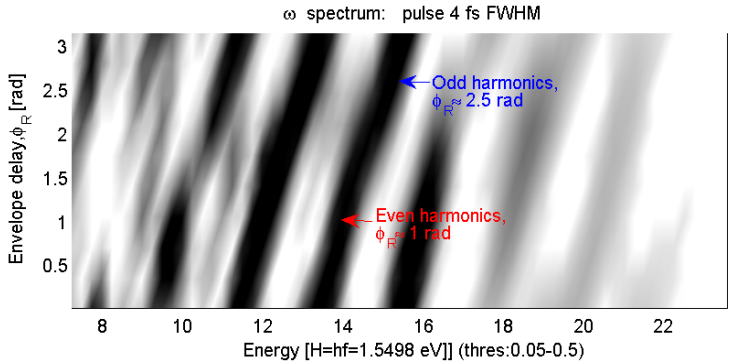

Figure 5.13: The harmonics from an ultra short IR pulse can be tuned from odd to even by changing the C-E phase, ϕ_R.

$\omega/2\omega$-pulses

Having found the optimal C-E phase for single attoburst generation using IR pulses, the generation is optimized with an additional 2ω field:

$$A(t) = A_0 \left(\cos(\omega t + \phi_R) + \xi_A \cos(2\omega + \phi_B)\right) \times \Lambda_N(t),$$

where $\xi_A \approx \xi/2 = E_B/2E_R$ is the relative amplitude of the two vector potentials and ϕ_B is the delay of the 2ω field relative to the envelope Λ_N. Even with this very ideal description of the pulse, there is a large number of parameters that can be tuned to optimize the generation:

Envelope duration	N
IR intensity	I_R
Relative intensity	$\mathcal{R}_I$
C-E delay	ϕ_R
2ω delay	ϕ_B
High pass filter	H_{hp}

where $\mathcal{R}_I = \xi^2$ is the relative intensity. We set $\phi_R = 0.8$ rad, because it is reasonable to assume that this delay will be remain optimal for weak relative intensities[3]. The IR intensity is set to 2×10^{14} W/cm^2 and relative intensities are studied from 1% to 40%. We find that the optimal 2ω delay is contant for all studied relative intensities:

$$\phi_B \approx 3 \pm 0.1 \text{ rad}.$$

This delay corresponds to a single trajectory at the end of the plateau, and multiple trajectories in the cut off. Figure 5.14 and Figure 5.15 shows that

[3]This was later verified to be true.

the optimal generation occurs when the cut off is located at the lowest possible energy. The peak intensity of the bursts increases strongly with the relative intensity. It is possible that the increase in intensity is exaggerated in the SFA model because it does not include any saturation effects due to ionization. The results agree qualitatively with recent experiments in Lund [4]. More experiments, with locked relative delays, must be made to verify this result.

The intense bursts that are produced by the $\omega/2\omega$ pulses, with $\phi_R \approx 0.8$ and $\phi_B \approx 3$, are not shorter than those of the IR pulses. The effective amount of bandwidth remains the same for the two different pulses. The bandwidth can be increased by choosing a different value of ϕ_B, see Table 5.1. This is demonstrated in Figure 5.16, where $\phi_B = 0$ and a long smooth second plateau is created.

Pulse duration [as]	Transform limited	With phase
IR	241	261
$\omega/2\omega$	125	180

Table 5.1: The duration of the single attosecond burst can be reduced using a special synchronization of the $\omega/2\omega$ field.

It is interesting to compare the $\omega/2\omega$ spectra with those of IR- and 2ω pulses, see Figure 5.17. The shape of the $\omega/2\omega$ spectrum can be explained as a combination of the ω- and the 2ω spectra: The ω spectrum has low intensity but high cut off energy; while the 2ω spectrum has a high intensity but a low cut off energy. High burst intensity can be realized when the beams are synchronized so that we can create a single trajectory in the 2ω regime.

Single Bursts from 10 fs Pulses

Using a 2ω field we can generate single bursts from longer IR pulses. We need a relative intensity of at least 20% to generate single bursts from 10 fs pulses, see Figure 5.18. Increasing the relative intensity results in a cleaner burst and an elevated first plateau, see Figure 5.19. The optimal laser beam delays vary for different pulse durations. Using $\phi_R = 0.8$, the best generation is found for $\phi_B = 2.5 \pm 0.1$. Further optimization can be done, but we are satisfied with the conclusion that single bursts can be obtained using 10 fs laser pulses. It does not seem possible to single bursts from $\omega/2\omega$ pulses when the pulse duration is longer than 10 fs.

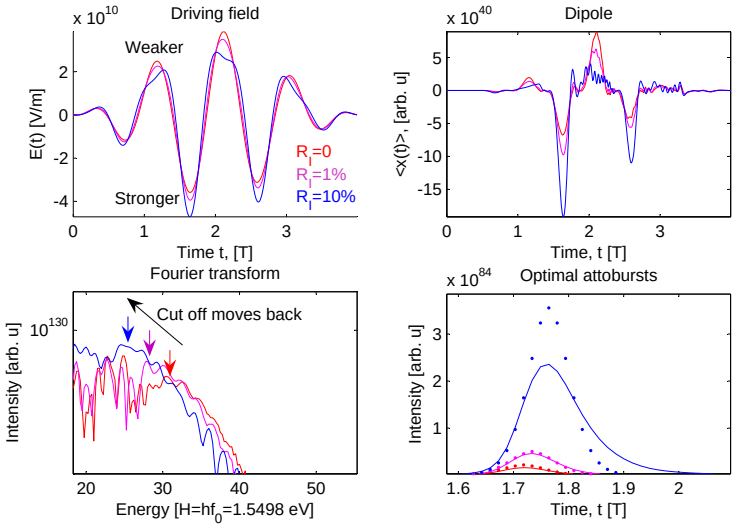

Figure 5.14: Using a 2ω field we can greatly improve the harmonic generation and the intensity of the attoburst. The dotted bursts are transform limited.

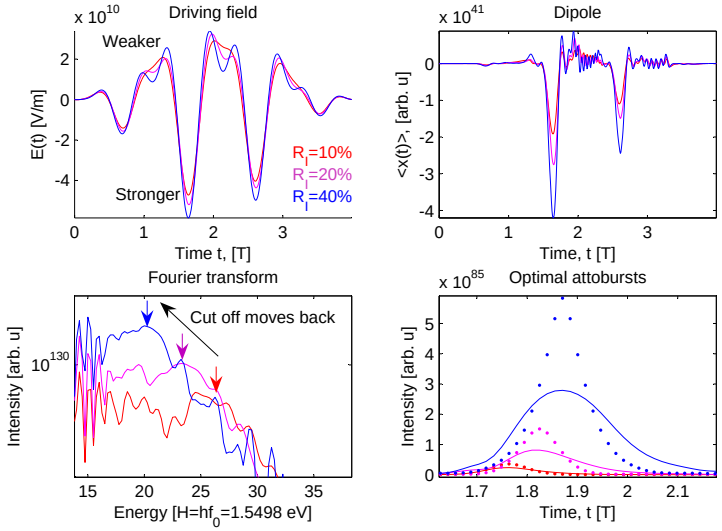

Figure 5.15: Increasing the intensity of the 2ω field and tuning the relative delays can dramatically increase the attoburst intensity. The dotted bursts are transform limited.

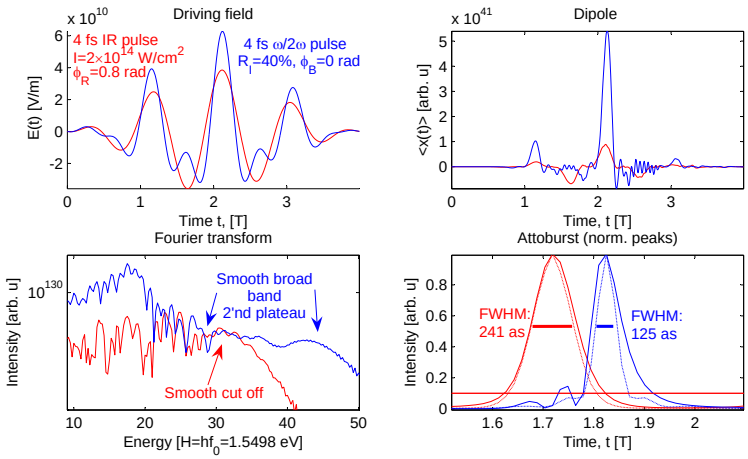

Figure 5.16: Using a special delay for the 2ω field, $\phi_B = 0$, a long smooth second plateau is generated (blue line). This generation process is very similar to the one in Figure 5.4. The intensity is comparable to that of the IR, but the bandwidth is greatly improved. The transform limit states that broad bandwidth implies short bursts. In the attoburst plot, we see that the pulse duration is almost reduced be a factor of two.

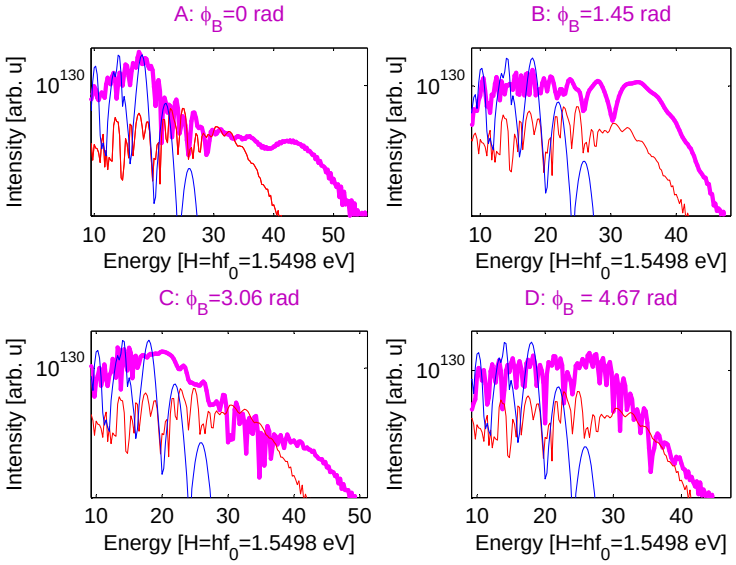

Figure 5.17: The $\omega/2\omega$ pulse (purple) is compared to a ω pulse (red) and a 2ω pulse. The spectrum can be remodelled to resemble either the 2ω- or the ω generation by tuning the ϕ_B delay. The cut off decreases when the intensity is optimized because the spectrum approaches the 2ω shape.

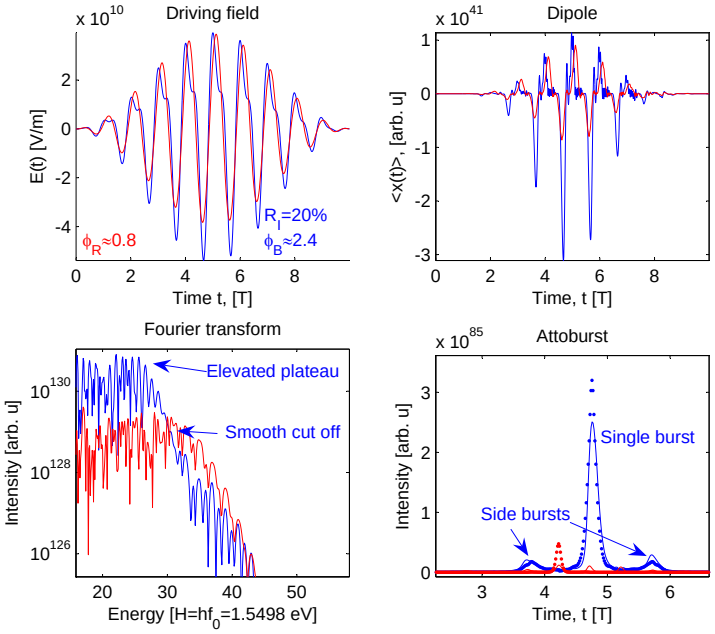

Figure 5.18: Single bursts can be produced from 10 fs $\omega/2\omega$ laser pulses if the 2ω field has an relative intensity of 20%.

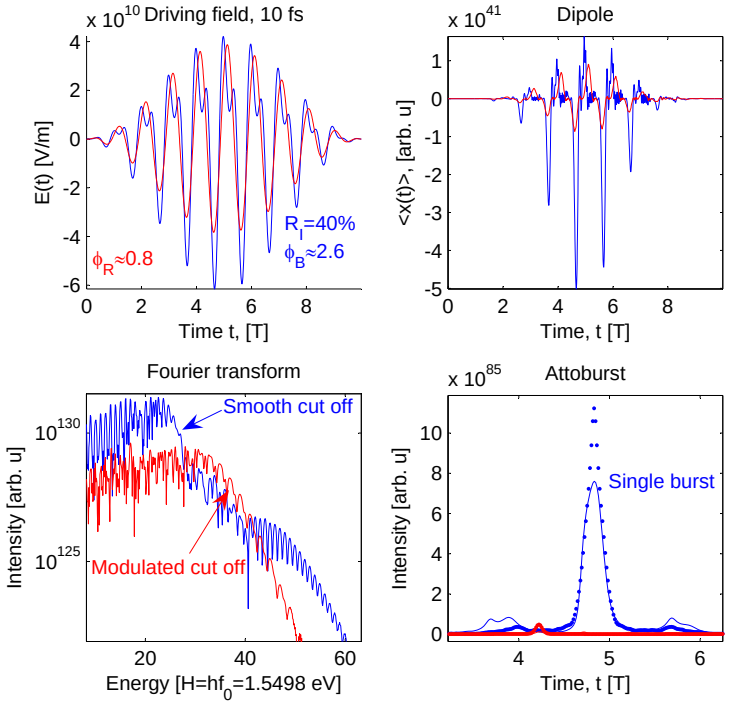

Figure 5.19: Increasing the relative intensity yields stronger single bursts.

Chapter 6

Discussion

High order harmonic generation (HHG) and attosecond electron dynamics has been studied intensely in the last decade. The generation of XUV attosecond bursts will become an important component of time resolved pump-probe experiments of atoms and molecules.

The strong field approximation (SFA) consists of a comprehensive mathematical framework that describes the HHG process in a nonperturbative manner. The main goal of this Thesis was to implement SFA in MATLAB so that the HHG can be calculated from arbitrary low frequency driving fields. The second goal of the Thesis was to study the properties of HHG with an $\omega/2\omega$ driving field. The atomic response depends on the relative intensity of the 2ω component which leads to a range of different applications.

6.1 Results

The HHG of a pure ω field results in two attosecond bursts per laser period. The corresponding spectrum consists of odd harmonics of the driving field. When the 2ω field is relatively weak, the $\omega/2\omega$ field can be used to make an in situ measurement of the harmonic phases of the pure ω field. We have shown that the RABBIT method produces the same trace as the in situ measurement for attosecond pulses generated by the SFA program.

Increasing the relative intensity of the $\omega/2\omega$ field completely alters the harmonic structure. Attosecond bursts are now generated once per period and the spectrum contains even and odd harmonics of the driving field. It is possible to fine tune the energy of generated attosecond bursts by simply adjusting the relative delay between the ω and the 2ω fields. This "tunability" will improve the quality of future pump-probe experiments.

Single attosecond bursts (SAB) can not be generated from ω driving pulses exceeding 5 fs. When $\omega/2\omega$ driving pulses are used, SAB can be generated from pulses as long as 10 fs. It is therefore clear that the $\omega/2\omega$ is the better choice when generating SAB. It has also been shown that the intensity of the burst can be increased significantly due to the influence of the 2ω field. The duration of the SAB can be reduced using a special synchronization of the $\omega/2\omega$ field. It is, however, not possible to combine the amplification and the compression properties.

6.2 Perspectives

The $\omega/2\omega$ field shows a lot of promise because it can increases the control and the intensity of the HHG process. The in situ measurement and the tunability have already been demonstrated experimentally. It would be interesting to take part in an experiment where the conversion efficiency and the tunability are optimized using phase locked $\omega/2\omega$ pulses.

The next step in the theoretical work is to study other kinds of polychromatic driving pulses. The $\omega/2\omega-\delta$ consists of two incommensurable frequencies which leads to new applications and phenomena. Also the effects of chirped polychromatic driving pulses will be studied. Because the SFA program is fully general, it is now straight forward to calculate the HHG of any low frequency field.

Acknowledgment

I want to thank everyone in the research group of "Attosecond Physics High-Order Harmonic Generation", at Lund Institute of Technology (LTH). I want to thank Johan Mauritsson for being an excellent supervisor and for presenting this exciting topic to me. Anne L'Huillier deserves many thanks for helping me with the details of the Strong Field Approximation and also for sending me to to Zürich, where I got some practical experience, and to Bonn, where I attended lectures on Ultra Fast Physics. Thanks to Per Johnsson for inspiring me to rewrite my MATLAB code, which ultimately made it run 100 times faster! I want to thank Erik Gustafsson for showing me his $\omega/2\omega$ experiment in Zürich and for providing housing. I want to thank Thierry Ruchon for constantly providing me with interesting reading material and for sharing his french humor. I thank Marko Swoboda for all the interesting coffee breaks and for a crash course in Inkscape; and I thank Thomas Remetter for running a RABBIT simulation on one of my theoretical attosecond bursts. I thank Miguel Miranda for reading though my Thesis and for his insightful comments. Thanks to Mikkel Brydegaard for sharing his views on Physics and Applications.

Bibliography

[1] D.J. Griffiths, "Introduction to electrodynamics", Prentice hall (1999)

[2] R.W. Boyd, "Nonlinear optics", Academic press (1992)

[3] J.L. Krause, K.J. Schafer, and K.C. Kulander,"High-order harmonic generation from atoms and ions in the high intensity regime", Phys. Rev. Lett. **68**, 3535 (1992)

[4] E. Georgiadou, "Study of harmonic generation with a two-color field"; Lund university, LRAP-375 (2007)

[5] J. Mauritsson, P. Johnsson, E. Gustafsson, A. L'Huiller, K.J. Schafer, M.B. Gaarde, "Attosecond pulse trains generated using two color laser fields", Phys. Rev. Lett. **97**, 013001 (2006)

[6] N. Dudovich, O. Smirnova, J. Levesque, Y. Mairesse, M.YU. Ivanov, D.M. Villenevue, P.B. Corkum, "Measuring and controlling the birth of attosecond XUV pulses", Nature physics 434 (2006)

[7] A. Baltuska, Th. Udem, M. Uiberacker, M. Hentschel, E. Goulielmakis, Ch. Gohle, R. Holzwarth, V.S. Yakovlev, A. Scrinzi, T.W. Hansch, F. Krausz, "Attosecond control of electronic processes by intense light fields", Letters to nature **42**, 611 (2003)

[8] Y. Oishi, M. Kaku, A. Suda, F. Kannari, K. Midorikawa, "Generation of extreme ultra violet continuum radiation driven by a sub-10-fs two color field", Optics Express **14**, 7230 (2006)

[9] M. Lewenstein, "Theory of high-harmonic generation by low-frequency laser fields", Phys. Rev. A, **49**, 49 (1994)

[10] P. Salieres, B. Carre, L. Le Deroff, F. Grasbon, G. G. Paulus, A. Sanpera, M. Lewenstein, "Feynman's path-integral approach for intense-laser-atom interactions", Science reports **292**, 902 (2001)

[11] L.N. Hand, J.D. Finch, "Analytical Mechanics", Cambridge University Press (1998)

[12] E. Cormier, P. Lambropoulos, "Optimal gauge and gauge invariance in a non-perturbative time-dependent calculation of above-threshold ionization", J. Phys. B: At. Mol. Opt. Phys. **29**, 1667 (1996)

[13] J.J. Sakurai, "Advanced quantum mechanics", Addison Wesley (1967)

[14] R.P. Feynman, "Space-time approach to non-relativistic quantum mechanics", Rev. of Mod. Phys. **20**, 367 (1948)

[15] M. Lewenstein, P. Saliers, A. L'Huillier, "Phase of the atomic polarization in high-order harmonic generation", Phys. Rev. A **52**, 4747 (1995)

[16] M. Lewenstein, A. L'Huillier, "Principles of single atom physics: High-order harmonic generation, above-threshold ionization and non-sequential ionization", Springer-Verlag, (in press 2007)

[17] H.A. Bethe, "Quantum mechanics of one- and two-electron atoms", Plenum (1977)

[18] M.Y. Ivanov, "Femtosecond science program", Steacie Institute of Molecular Sciences (Feb 21, 2002)

[19] J.J. Sakurai, "Modern quantum mechanics", Addison-Wesley (1994)

[20] P. Antoine, A. L'Huillier, M. Lewenstein, "Attosecond pulse trains using high-order harmonics", Phys. Rev. Lett. **77**, 1234 (1996)

[21] G. Sansone, E. Benedetti, C. Vozzi, L. Avaldi, R. Flammini, L. Poletto, P. Villoresi, C. Altucci, R. Velotta, S. Stagira, S. De Silvestri, M. Nisoli, "Isolated single-cycle attosecond pulses", Science rep. **314**, 443 (2006)

Appendix A

Matlab files

nydipol.m

The dipole moment is calculated using a dipole matrix ΔX and a mask matrix M. The dipole matrix contains the dipole integration elements Δx_{nm}; while the mask matrix determines the integration bounds for the dipole, see Figure A.1. The standard shape of M is given by:

$$M_{nm} = \begin{cases} 1, & n \in [n_0, \hat{n} - \hat{m} + n] \\ 0, & n \notin [n_0, \hat{n} - \hat{m} + n] \end{cases} ,$$

which corresponds to an integration from as far back as possible: t_0 to t_m, for all $m \in [1, \hat{m}]$. Specific electron trajectories can be studied if the mask marix is modified.

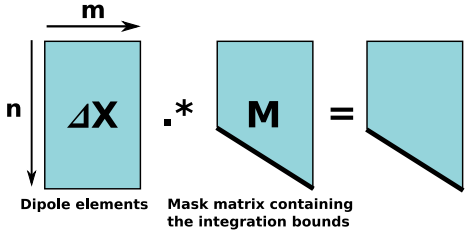

Figure A.1: The ΔX matrix contains all the matrix elements Δx_{nm}. We create a matrix M with a specific shape, so that the integration bounds are fullfilled when the rows are summed. Specific trajectories can be seleced by changing the shape of M.

The numerical integration is carried out by summing the rows of $\Delta X. * M$, which is a efficient to do with MATLAB [1].

The input parameters for NYDIPOL.M are: *startAt*, *endAt* and *saveAs*. If $startAt = a$ and $endAt = b$, then NYDIPOL.M will plot the dipole from IR period a to b. The calculated dipole is saved as SAVEAS.MAT or as QUICKSAVE.MAT if no specific filename is chosen.

[1] We denote elementwise multiplication of two matrices A and B as $A. * B$. The same notation is used in Matlab.

getConstants.m

Loads a bunch of physical constants into a global vector *CONSTANTS*:

CONSTANTS(1)	T	Period of IR
CONSTANTS(2)	ω	Ang. freq. of IR
CONSTANTS(3)	A_0	Ampl. of vector potential
CONSTANTS(4)	I	Intensity
CONSTANTS(5)	I_p	Ionization potential
CONSTANTS(6)	e	Unit charge
CONSTANTS(7)	c	Speed of light
CONSTANTS(8)	m	Electron mass
CONSTANTS(9)	$\hbar$	Dirac's constant
CONSTANTS(10)	ν	Integration paramter
CONSTANTS(11)	U_p	Ponderomotive energy

explicitA.m

The vector potential $A(t)$ is used to describe the driving field.

fouriertransform.m

A file saved by NYDIPOL.M is loaded and the Fourier transform of the dipole moment is calculated using the FFT routine in Matlab. The spectrum is passed through a high pass filter, starting at harmonic H_{hp}, and then transformed back to the time domain.

The input parameters are *startAt*, *stopAt*, *fileToLoad* and *gcol*, where the first two arguments should be 0 and $b - a$ for maximal resolution. The harmonic spectrum and the pulse structure is plotted in the color specified by *gcol*.

spectrum.m

A super function, called SPECTRUM.M, is used to run NYDIPOL.M and FOURIERTRANSFORM.M multiple times, for varying input parameter values of the driving field. The result of the simulation is saved and can be viewed using STUDYSPECTRUM.M.

The input parameters are *NEL*, *startAt*, *endAt* and *saveAsSPEC*, where *NEL* specifies the number of simulations to produce.

studySpectrum.m

A file saved by SPECTRUM.M is loaded and plotted.

Appendix B

Poster

Attoburst Generation in Bichromatic Fields – Tunability and Quantum Path Engineering

M. Swoboda & M. Dahlström, M. Miranda, E. Gustafsson, T. Remetter,
T. Ruchon, E. Georgiadou, J. Mauritsson, A. L'Huillier
Department of Physics, Lunds Universitet, P.O. Box 118, 22100 Lund

Introduction

Here, we present calculations in the Strong-Field-Approximation and corresponding experiments on High-Order Harmonic Generation with bichromatic driving laser fields. A fraction of the initial infrared pulse is frequency-doubled and overlapped with the fundamental beam in the generation gas, showing great influence on the harmonic emission temporal and spectral properties.

Two-Color Fields in HHG

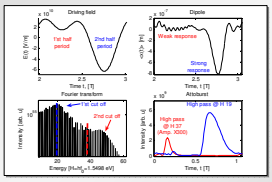

We break the inversion symmetry using an additional 2ω field in High-Order Harmonic Generation[1]. This enables us to generate single bursts of harmonic radiation per driving laser period. The shape of the harmonic spectrum is altered, showing a structure of two plateaus. They are the result of the different harmonic generation efficiencies of the two frequencies, where the high-gain-but-low-energy cutoff is corresponds to the 2ω plateau.

Experimental Setup

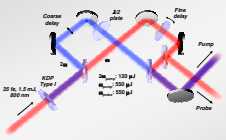

Using a two-color Michelson interferometer, the frequency doubled output of our Ti:Sa laser system is superposed with 800 nm radiation in the generation gas cell. The relative phase of the fields can be altered, as well as their intensity. For detection, we use a Mach-Zehnder interferometer, where a fraction of 800 nm light is used to streak photoelectrons from our as-pulse train, which is visible on our velocity-map imaging spectrometer.

Harmonic Spectrum

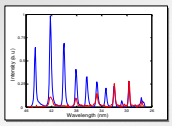

The intensities of high harmonic combs generated with either a single- or two-color field are compared.
Both spectra extend to roughly the same harmonic order, but with the two-color field (blue spectrum), the intensity of the lower order harmonics is greatly increased.
The two plateaus are visible as the cutoff of the increased-efficiency region, mentioned already to the left. The High-Order Harmonic Generation efficiency is greater at a frequency of 2ω.

SFA Calculated ω/2ω Relative Phase

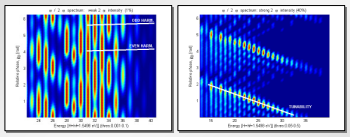

The harmonic generation can be tuned from even to odd harmonics using the 2ω driving field (1% relative intensity)[3]. The 2ω field extends the quantum paths of one half infrared (IR) period and diminishes the other. Due to the perturbation, the paths accumulate different phases in the continuum, leading to the observed interferences with relative delay. The central energy of the attobursts can be fine-tuned using stronger 2ω driving fields(40% relative intensity). Also, the strong dominance of one quantum path per period leads to the emission of only attosecond pulse per IR cycle.

Experimental ω/2ω Relative Phase

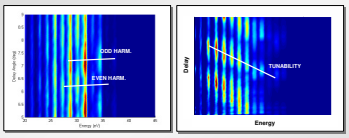

The experimental results show good correspondence with the SFA calculations on the left. We control whether odd or even harmonics dominate the spectrum when the 2ω intensity is low. Tunability of the harmonic central energy is shown on the right for higher relative 2ω intensity .

Streak Camera Experiment

We employ the measurement principle of an attosecond streak camera [4] to measure the time evolution of the probing IR field.
The scan is the cut of the central line of a sequence of velocity maps, obtained for different delays between attosecond pulse train and probe IR. The vector potential of the IR probe will then alter the observed photoelectron spectrum.
The intrinsic chirp [5] of the harmonic emission is visible in the imbalance of rising and falling edge of the oscillation, visible also as a 180 degree shift between upper and lower harmonic spectrum.

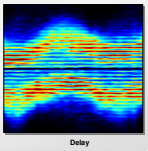

A Quantum Stroboscope

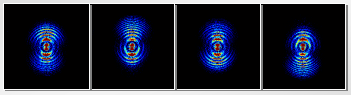

The one pulse/IR cycle attotrain allows the stroboscopic measurement of electron wave packet scattering on its parent ion. A single ionization instant can be frozen in time and the electron afterwards steered by the probing IR field. The subsequent electron wave packets are coherent and add up in phase, increasing the signal by n^2 [3].

References

[1] P. Johnsson *et al.*, Phys. Rev. Lett. **97**, 013001 (2006)
[2] J. Mauritsson *et al.*, *manuscript in preparation*, (2007)
[3] N. Dudovich, Nature Physics, **2**, 781 (2006)
[4] R. Kienberger *et al.*, Nature (London) **427**, 817 (2004)
[5] Y. Mairesse *et al.*, Science **302**, 1540 (2003)

Conclusions

In conclusion, two-color driving laser fields present a viable and efficient method to control the harmonic emission temporal and spectral structure, allowing the production of tunable attosecond pulse trains with one pulse per IR cycle.
The tunability is a consequence of the engineered electron quantum paths in the continuum. Two cutoffs appear in the spectrum, and the dominance of either odd or even harmonics can be obtained by only a weak perturbing field at certain relative phase. We perform several experiments, using these pulse trains as a stroboscope to capture attosecond electron wave packet dynamics.